INTERPRETATION OF A SEISMIC REFRACTION PROFILE FROM THE RICHARDSON MOUNTAINS, YUKON TERRITORY

By

Simon O'Brien

B.Sc.(Hons) Geophysics, Memorial University of Newfoundland

A THESIS SUBMITTED IN PARTIAL FULFILLMENT OF

THE REQUIREMENTS FOR THE DEGREE OF

MASTER OF SCIENCE

in

THE FACULTY OF GRADUATE STUDIES

DEPARTMENT OF GEOPHYSICS AND ASTRONOMY

We accept this thesis as conforming

to the required standard

THE UNIVERSITY OF BRITISH COLUMBIA

April 1990

08

In presenting this thesis in partial fulfilment of the requirements for an advanced degree at the University of British Columbia, I agree that the Library shall make it freely available for reference and study. I further agree that permission for extensive copying of this thesis for scholarly purposes may be granted by the head of my department or by his or her representatives. It is understood that copying or publication of this thesis for financial gain shall not be allowed without my written permission.

Department of Geophysics and Astronomy

The University of British Columbia

129-2219 Main Mall

Vancouver, Canada

V6T 1W5

Date:

_____ May 2, 1990 _____

Abstract

In March of 1987, the Geologic Survey of Canada conducted a major seismic refraction experiment in the Mackenzie Delta-Southern Beaufort Sea-Northern Yukon area. This study involves the analysis of a portion of the resulting data set. A 2D velocity profile through the Richardson Mountains of the northern Yukon has been constructed using raytracing to model the travel-times and amplitudes. The line is approximately 320 km long, running from a shotpoint on the Eagle Plains in the south to one 50 km offshore in Mackenzie Bay to the north, with an average receiver spacing of 3.5 km. An additional shotpoint is located at Shingle Point, on the shore of Mackenzie Bay.

A series of four sedimentary basins separated by major structural highs produces a complex basement structure. Two distinct upper crustal layers were modelled, a 5.95 km/s layer overlying a 6.3 km/s layer, as well as a lower crustal layer with a velocity of 7.25 km/s. Crustal velocity gradients are low (≤ 0.005 s^{-1}). The 6.3 km/s layer pinches out beneath the Beaufort-Mackenzie Basin in the north, accompanied by a thinning of the lower crust from a thickness of 20 km in the south to less than 10 km beneath MB. This results in the crust as a whole thinning from a thickness of 50 km under the Richardson Mountains to only 40 km under the Beaufort-Mackenzie Basin. The velocity of the upper mantle is 7.95 km/s.

The modelling of shear wave arrivals indicate Poisson's ratios of 0.23 ± 0.02 in the upper crust and 0.25 ± 0.02 in the lower crust.

Table of Contents

List of Tables

List of Figures

Acknowledgement

Chapter 1

GEOLOGY AND TECTONICS

1.1 Introduction

In order to determine deep crustal structure in the Mackenzie Delta-Southern Beaufort Sea-Northern Yukon area, the Institute of Sedimentary and Petroleum Geology of the Geological Survey of Canada conducted a major seismic refraction experiment in March of 1987, with the participation of the Geodetic Survey of Canada and the Universities of British Columbia and Calgary. The survey consisted of three lines having a total length of 940 km, as shown in Figure 1.1. A complete description of the experiment is provided in Stephenson et al. (1989). This thesis involves the modelling of the velocity structure for line C using an asymptotic ray theory algorithm to interpret the travel-times and amplitudes, with surface geology as the primary additional constraint. The main objectives of this study were to determine the crustal velocity structure in the area and to provide answers to several of the many regional tectonic questions which remain unanswered.

In contrast to the surrounding plains, which have undergone considerable petroleum exploration, the Richardson Mountains area of the northern Yukon has seen little activity in the earth sciences. Geological data have been collected and compiled into 1 : 250 000 scale geologic maps but little structural analysis has been done, and consequently elemental problems such as the direction and amount of movement on some of the major faults remain unsolved. Geophysical information is even more sparse, with gravity being the only regional data set containing deep crustal information. Thus there are few constraints governing the
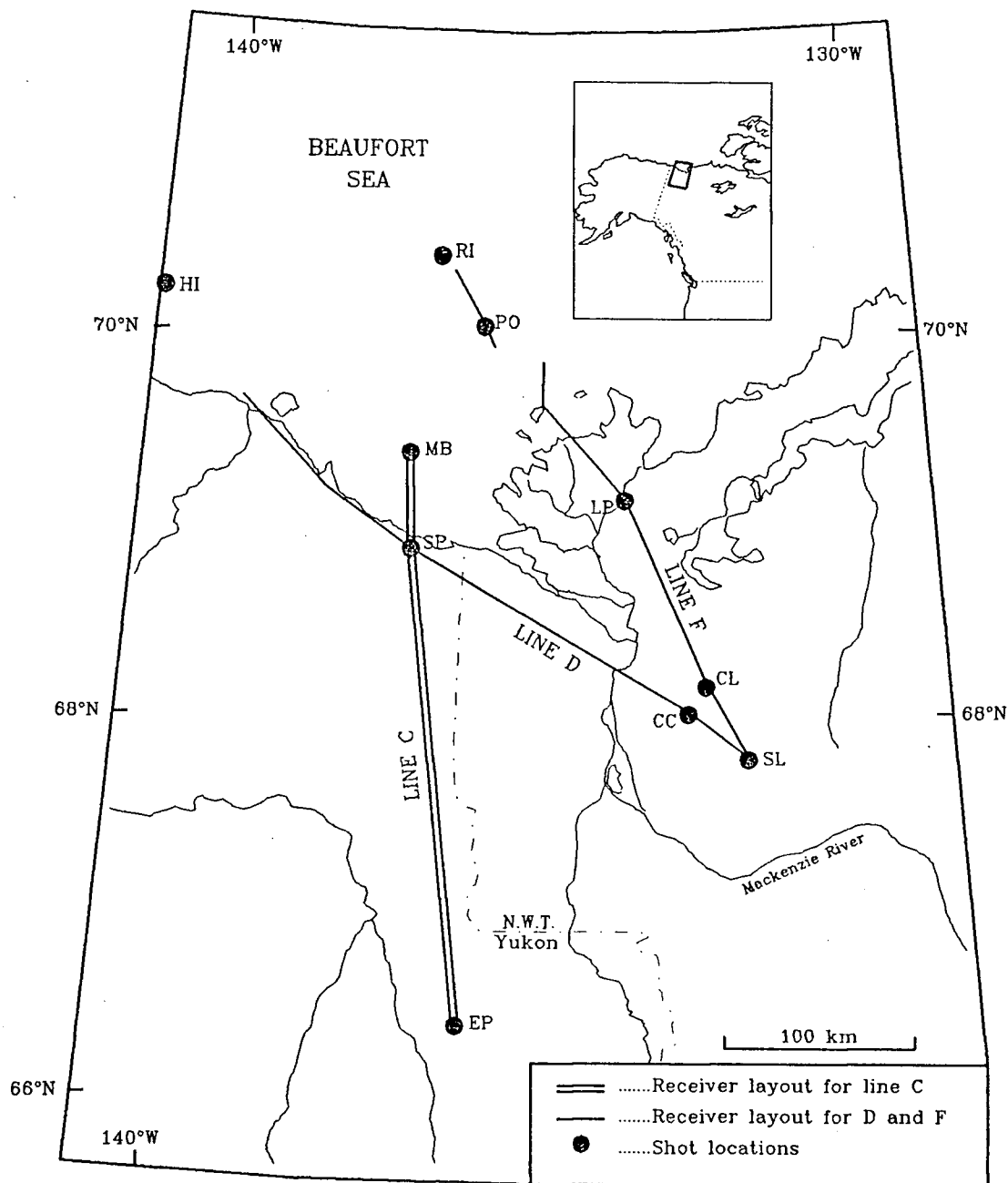
1

Figure 1.1: Layout of the Mackenzie Delta-Southern Beaufort Sea-Northern Yukon seismic refraction experiment. Inset shows the location of the survey area.

tectonic models for the region.

1.2 Tectonic models

The tectonic history of the Mackenzie Delta-Southern Beaufort Sea-Northern Yukon area clearly involves the interaction of the North American and Eurasian continental plates, however, debate exists about the form of this interaction. Due to the lack of detailed structural data, the tectonic models which have been proposed are largely speculative, based primarily upon large scale surface geology. A number of radically different models have been proposed. These generally fall into one of two basic groups; those which involve the movement of Alaska along major strike-slip fault systems and those in which Alaska rotates away from the Canadian Arctic due to sea floor spreading in the Canada Basin (Figure 1.2).

The rotation models differ only in the amount of the basin opened by spreading. Although Grantz et al. (1979) suggested that the entire Canada Basin was opened by rotational spreading starting early in the Jurassic, the more conventional view is that spreading was confined to the southern part of the basin, and that the northern part is of older origin. Churkin and Trexler (1980), for example, proposed that the northern part of the basin was part of a 'proto-Pacific' plate which was isolated during the Jurassic when the 'Kolyma' plate plugged the gap between Alaska and Siberia. Paleomagnetic data indicate that northern Alaska rotated 70° relative to the Canadian arctic during the Mesozoic (Irving,1977) with the rotation beginning in the Jurassic. Epicontinental sedimentation in the Beaufort-Mackenzie Basin ended early in the Cretaceous, with subsequent sediments being of fluviodeltaic origin (Young et al., 1976). This suggests that spreading ceased during the Early Cretaceous. Using sparse gravity data, Grantz et al. (1979) inferred the location of an inactive ridge in the southern Canada Basin (see Figure 1.2). The analysis of equally sparse aeromagnetic data by Taylor et al. (1981) indicated approximately the same ridge position, while Vogt et
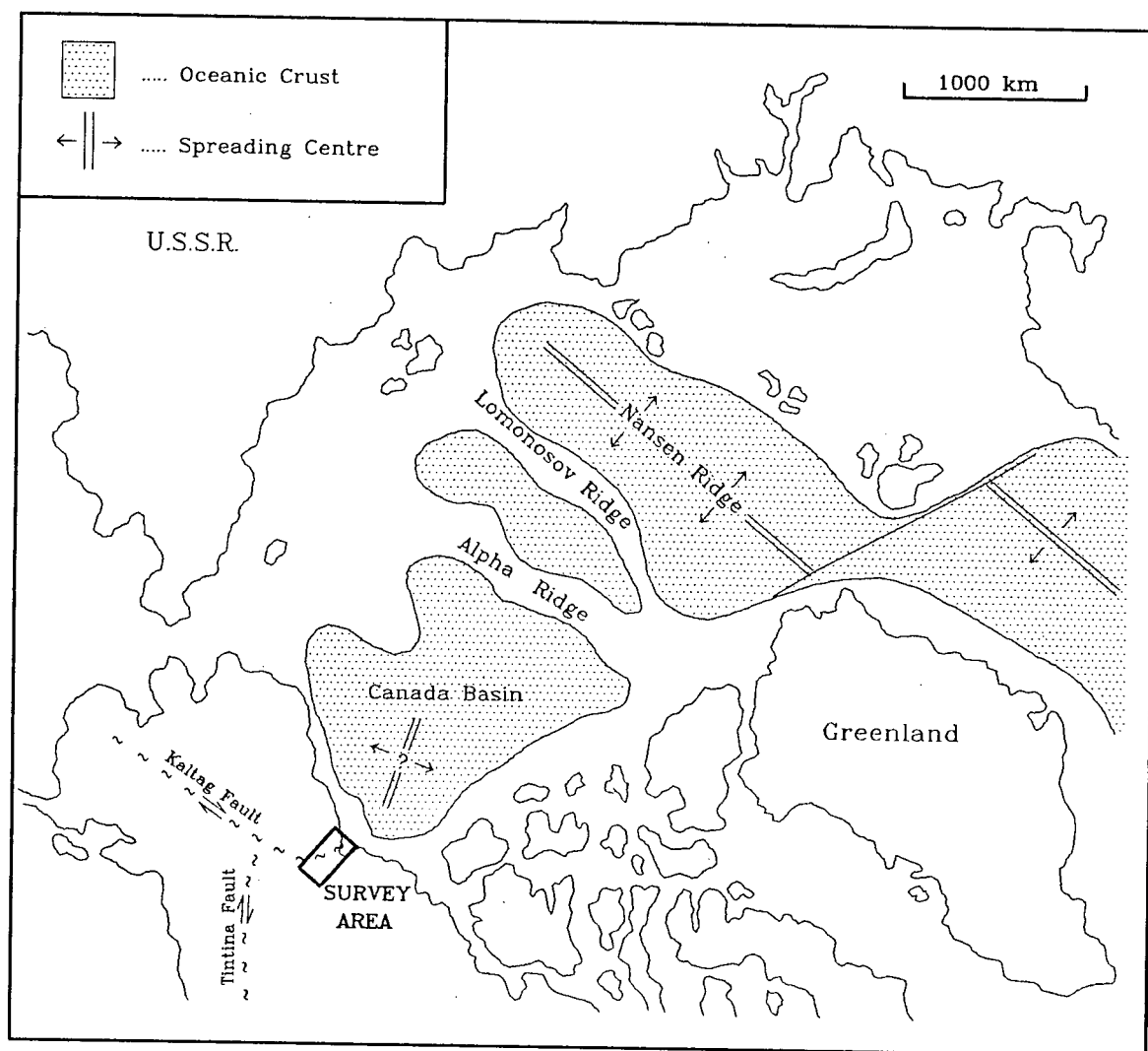
Figure 1.2: Structural features in the Arctic Ocean basins and adjacent areas, showing the location of the survey area.

al. (1982) showed that the same data could be interpreted to indicate a number of possible spreading centre locations. Even now, however, there is no entirely convincing evidence for a spreading centre in the basin.

The fault based models vary considerably. Using palinspastic lithofacies reconstruction, Jones (1980) suggested that northern Alaska was positioned adjacent to southern Yukon in the Permian but moved hundreds of kilometres to the north along the Tintina fault and then rotated along the Kaltag fault into its present position during the Triassic. Dutro (1981) proposed that Alaska rifted off northern Europe and moved across the arctic along the coast of the Canadian arctic islands as a result of sea floor spreading at the Alpha and Nansen Ridges, while Herron et al. (1974) suggested that northern Siberia rifted off the Canadian arctic islands and moved westward along a shear zone parallel to the northern Alaska coastline. The model of Churkin and Trexler(1980) included the movement of northern Alaska to the northeast along the Kaltag fault, initiated by a collision of the North American plate with the Siberian 'Kolyma' plate.

There are a number of problems with the fault-based theories. It is doubtful that the Alpha Ridge was ever a spreading centre. Weber and Sweeney (1985) showed that the density structure of the Alpha Ridge is similar to that of the Lomonosov Ridge, which is known to be of continental origin (Sweeney et al., 1982). If the Nansen Ridge were responsible for the 4000 km of spreading required by Dutro (1981), a major subduction zone would be required in northern Europe and Siberia for which there is no evidence. Lane (1988) suggests that the Kaltag-Rapid fault array in the northern Yukon is actually a compressional fold belt and that little, if any, strike slip motion has occurred in the Richardson Mountains area. The model of Jones (1980) is therefore unlikely. In addition, seismic reflection data from the continental margin north of Alaska (Grantz and May, 1983) showed no evidence of a major shear zone. The proposal of Churkin and Trexler (1980) may still be viable, since it does not require as much motion on the Kaltag fault and because the major bend on this fault in the

Yukon, from a northeasterly trend to a northerly trend, would cause the motion to be more compressional than strike-slip in the northern Yukon.

1.3 Tectonic elements

Although the tectonic history of the Richardson Mountains is not well understood, it is possible to divide the area into a number of smaller regions which have distinct structural characteristics. These 'tectonic elements', first introduced by Norris (1974), are shown in relation to line C in Figure 1.3. In the south is the Richardson Anticlinorium, a horst-like structure which exposes Cambrian to Devonian sediments which dip gently to the north. The near-vertical Deception Fault separates this element from the Eagle Fold Belt, a sequence of Jurassic and Cretaceous sediments which have undergone mild Laramide deformation. To the north of this are the White and Rat Uplifts, where Cambrian to Permian sediments are exposed by a complex combination of folding and faulting. They are part of the north-easterly trending series of small local uplifts known as the 'Aklavik Arch Complex', which is believed to have formed at least in part by late Paleozoic compressional deformation (Cook et al., 1987).

The Eskimo Lakes Fault Zone marks the boundary between the Aklavik Arch and the Rapid Depression, a small basin containing up to four kilometres of Mesozoic sediments (Dixon et al., 1985). These sediments have been deformed by the Rapid Fault Array, a series of north-trending, high-angle faults which Lane (1988) described as predominantly compressional.

The Rapid Depression is a sub-basin of the much larger Beaufort-Mackenzie Basin. The main portion of the Beaufort-Mackenzie Basin contains a very thick sequence of Mesozoic and younger sediments. Because of the high potential for oil and gas in the basin, it has been studied extensively by the petroleum industry, and hence the sediment structure is fairly well
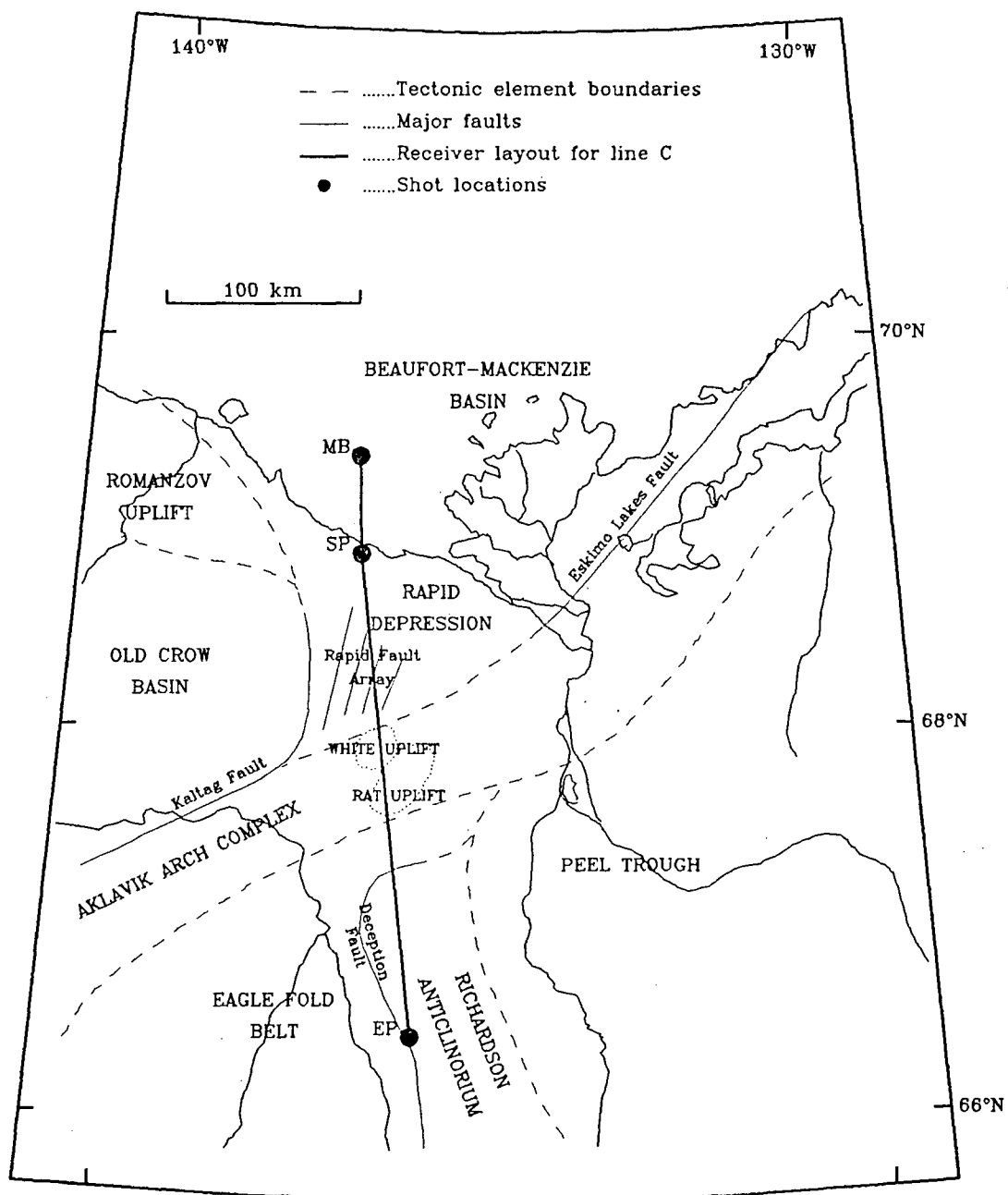
Figure 1.3: Tectonic elements in the northern Yukon.

known. Seismic reflection data show that there are up to 12 km of Jurassic to Quaternary aged sediments.

Middle to Upper Cambrian dolomites and limestones are exposed at the White Uplift, but the remainder of the section consists mainly of clastics. Upper Cambrian to Middle Devonian sediments are basinal shales, siltstones and sandstones, while the Upper Devonian is dominated by marine shales with some fine grained sandstones. These are unconformably overlain by Permian shales which contain some interbedded carbonates (Norris, 1984). There is the suggestion of another substantial unconformity in the Early Jurassic, with Upper Permian and Triassic sediments having been removed (Dixon et al., 1985). The Jurassic and Early Cretaceous sediments of the Beaufort-Mackenzie Basin consist primarily of shallow marine clastics, with a gradual facies change to alluvial and coastal plain sediments, including some coarse sandstones and conglomerates, occurring at the beginning of the Cretaceous (Young et al., 1976). The Middle Cretaceous consists of up to four kilometres of interbedded clastics, mostly Albian flysch (Dixon et al., 1985). The Middle Eocene is thought to have been a period of extensive uplift and erosion on the Yukon coastal plain, with 6 to 7 km of sediment having been removed (Majorowicz and Dietrich, 1989). However, deposition in the Beaufort-Mackenzie Basin has since continued at a fairly rapid rate, with at least two kilometres of deltaic sediments having been deposited during the Quaternary.

1.4 Study Objectives

The main purpose of this experiment was to determine the crustal velocity structure for northern Yukon, and therefore to provide new constraints upon the tectonic models discussed in Section 1.2. More specifically, there were four primary objectives:

1. to determine the crustal velocity structure beneath Mackenzie Bay and northern Yukon in order to constrain the nature of the continent-ocean transition.

2. to determine crustal velocity and thickness variations across the Kaltag Fault to see whether there is any evidence of crustal scale movement on the fault.

3. to examine the structure of the upper crust in order to determine the deep structural expression of sedimentary basins and major uplifts.

4. to provide velocities for use in the processing of seismic reflection data.

By examining how these constraints relate to the proposed tectonic models, and by comparing the velocity structure of the continental margin here to that of well studied margins elsewhere, the margins of the North Atlantic in particular, it was hoped that the tectonic history of this margin could be better determined.

Chapter 2

THE REFRACTION EXPERIMENT

2.1 Data Acquisition

2.1.1 Line layout and spacing

The Mackenzie Delta-Southern Beaufort Sea-Northern Yukon seismic refraction experiment was conducted in March of 1987 by the Institute of Sedimentary and Petroleum Geology, a division of the Geological Survey of Canada, using funding from the Frontier Geoscience Program. Participants included the University of British Columbia, which was involved in the deployment of receivers and the detonation of some shots, as well as the University of Calgary and the Geodetic Survey of Canada, which were responsible for surveying the offshore shot and receiver sites.

The experiment consisted of 10 shotpoints which were recorded along three lines, as shown in Figure 2.1, with an average receiver spacing of about 3 km. Line F ran approximately 300 km northwest from shot point SL on the Anderson Plain, across the Mackenzie Delta onto the ice of the Beaufort Sea. Line D ran about 320 km west-northwest from the shot point SL across the delta and the Yukon Coastal Plain, while line C ran 320 km north to south from shotpoint MB in Mackenzie Bay through shot SP on shore at Shingle Point to shot EP on the Eagle Plains. This layout resulted in the collection of approximately 830 km of reversed and 110 km of unreversed data as well as an additional 650 km of broadside data.

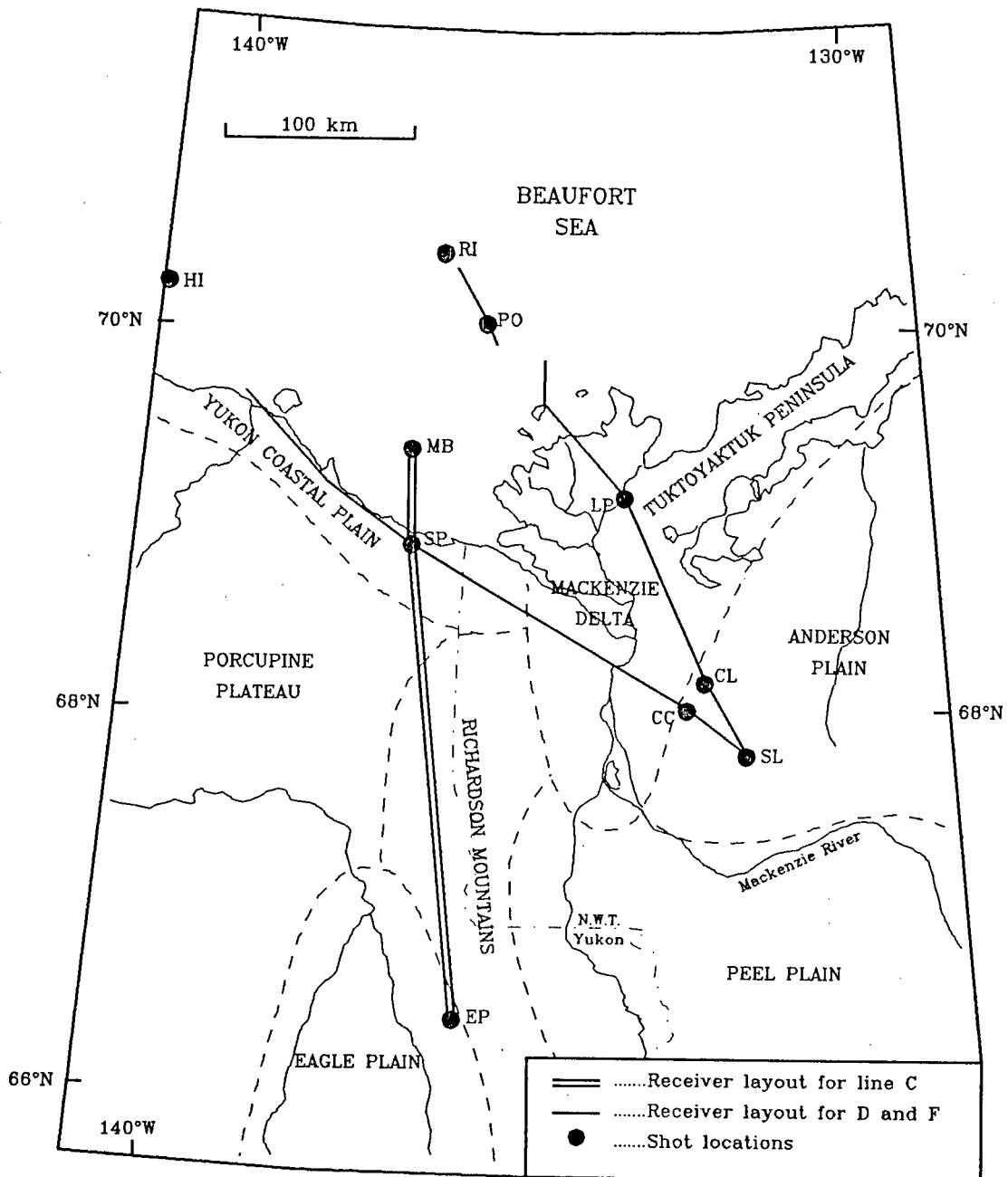Only the in line shots of line C (EP, SP and MB) will be discussed here, as they are the

Figure 2.1: Geography of the northern Yukon showing the layout of the experiment.

sole concern of this thesis. The primary objectives of this line were to determine the crustal thickness of the northern Yukon and to determine the crustal velocity structure, as discussed in Chapter 1. The resolution of the data, although sufficient to image very broad scale crustal features, is not adequate to provide near-surface detail, due to the receiver spacing of 3.5 km and the lack of intermediate shots between SP and EP.

2.1.2 Deployment and locating

A maximum of fifty-four Portable Refraction Seismographs (PRS's) were available at any one time, and consequently two separate layouts were needed for line C in order to obtain the desired coverage. Deployment of the recorders was from helicopters, while transportation of the shooters and explosives to the offshore sites was by Twin Otter. The onshore receiver site locations were determined using NTS 1 : 50 000 air photo maps or topographic maps, while offshore sites were located using Global Positioning System (GPS) satellite data. Since the offshore sites for line C were all on landfast ice, they could be surveyed without concern of ice movement. Shot sites at MB and SP were located using GPS while shot EP was located using the 1 : 50 000 maps and air photos. Positioning errors for all sites are thought to be less than 100 m. Onshore elevations were obtained from topographic maps, with errors in the order of 25 to 50 m.

2.1.3 Shot points

The explosive used at all shot points was Geogel 60% in 4.5 kg, 75 mm diameter charges as it was available in Inuvik at the time of the experiment. At the onshore sites EP and SP, the charges were placed into 30 m drill holes of 112 mm diameter. Each hole contained 90 to 99 kg of explosives with a tamped upper collar of at least 14 m, with reinforced detonating cord piercing the uppermost charge. The holes were arranged in five hole pentangular groups

SHOT	CHARGE SIZE (kg)
EP (near offsets)	1089
EP (far offsets)	2736
SP (near offsets)	495
SP (far offsets)	1386
MB (near offsets)	675
MB (far offsets)	1431

Table 2.1: Charge sizes used on line C.

with a minimum spacing of 30 metres between holes. Detonating cord and multiple blasting caps were used to join and synchronously detonate the desired number of shot holes. At the offshore site MB, the explosives were tied together using rope to obtain the desired charge sizes and loaded through the ice onto the sea floor, at a depth of 30 m, within a day of the shooting. To obtain a better signal-to-noise ratio at the more distant receivers, much larger charges were used for recording the far offset traces than were used for the near traces (see Table 2.1).

2.1.4 Receivers and timing

The data were recorded digitally by PRS's with 2 Hz seismometers and compiled subsequently on 9-track digital tapes using the Lithoprobe Data Storage format, a variation of SEG-Y (Spencer and Asudeh, 1987). The PRS's recorded 120 samples per second, starting one second before the shot time and continuing for two minutes, to give a total of 14 400 data points per trace.

The internal clock of each instrument was synchronized prior to each deployment to a clock receiving time code from the Geostationary Orbiting Environmental Satellite (GOES). Upon recovery the clocks were rated against the GOES clock to measure the time drift. Timing corrections were subsequently applied. Drifts were generally less than 10 ms, only

slightly longer than the sampling interval. Accurate shot times were obtained by using a chronometer-generated firing pulse, with the shooting clock also being set and rated against the GOES clock.

2.2 Data Processing

2.2.1 Preliminary processing

All processing and modelling were performed on the MicroVAX II computer in the Geophysical Research Processing Facility of the Department of Geophysics and Astronomy. A number of preliminary processing steps were required to prepare the data for analysis. The traces for each shot were sorted by their shot-receiver distances, which were calculated from latitudes and longitudes using spherical geometry. This projected the data onto the line of the model profile along circular arcs whose common focus was at the shotpoint. The maximum projection was 8 km, but 90% of the receivers were within 3.5 km of the line. The DC component of each trace was removed and noise spikes were edited out by resetting the value of the spiked data points to the average of the two adjacent data. For presentation purposes, the records from shot MB were muted starting at the onset of the high amplitude water arrival. Finally, since only a fraction of each trace actually contained significant arrivals, a 20 second window was applied to the data, starting on each trace at a time equal to the distance from the shot divided by 8 km/s. This reduced the amount of data and enhanced the time structure by increasing the slope difference between events of similar velocities.

2.2.2 Picking the arrivals

A number of steps were involved in the picking of the events. The first was to pick the obvious first arrivals by simply looking at each trace in turn and determining when the first motion occurred. To do this, the data were scaled to a common maximum amplitude in

order to view all of the first arrivals at once. This facilitated the identification of trends, and provided a time window in which to look for the first arrivals on the noisier traces. Picking was easy on the near-source traces, where the first arrivals were from the sediments or the upper crust and had a signal-to-noise ratio of at least two or three. At greater distances, where the first arrivals were much lower amplitude, the signal-to-noise ratio dropped below one on most traces and filtering was required.

To determine which filters would best enhance the data, frequency analyses were performed. By comparing the amplitude spectra for a part of the trace which contained only noise (i.e. before the first arrival) to a portion which did contain signal, it was possible to isolate the main frequency range of the signal itself. A bandpass filter designed to encompass this range was then applied to the data set. Traces which were still too noisy to pick were refiltered with more restricted pass bands. When no degree of filtering could enhance a distinguishable signal, the trace was left unpicked. Filtering was performed in the frequency domain using a simple trapezoidal function. Each filter was defined in terms of its four corner frequencies. Between the middle two frequencies it was assigned a value of 1.0, while outside the end frequencies it was assigned a value of 0. There was a linear transition between these two regions. Transition zone widths were chosen carefully to minimize the ripples resulting from the sharp corners of the filter.

Finally, each pick was displayed on the unfiltered data in order to determine whether the filtering process had obscured the arrival onset and to be sure that there was evidence of an arrival on the original trace. If there was not sufficient evidence for the pick, it was discarded. Some adjustment, generally less than 50 ms, was required of several of the picks of very low amplitude arrivals.

The errors involved in picking the near-source first arrivals were very small. The onset of the wavelet was generally clear, so it is unlikely that the picking errors were greater than 25 ms (approximately 3 data points). Further from the source, the errors increase to about 50

ms for lower crust refractions and may be as large as 100 ms for some of the low amplitude mantle arrivals and for arrivals from noisy traces.

Secondary picks were generally much more difficult to make. Even when there was a very sharp secondary arrival, the reverberations from the primary arrival tend to mask the onset. As a result, the errors associated with the secondary picks are estimated to be comparable to those from the noisy first picks, ranging from 50 to 100 ms.

2.2.3 Data scaling

Several scaling steps were required before the amplitudes could be analyzed. When the two data sets for each shotpoint were merged, a scale factor was determined to account for the difference in charge size. Due to the rapid decrease of amplitude with distance, the traces were also scaled by a function of distance to enable the display of events on the far traces. Finally, amplitude anomalies which were obviously caused by near surface structures, which were beyond the resolution of this survey, had to be suppressed.

The far traces for each shot point were obtained using a much greater charge than the near traces (Table 2.1). It was therefore necessary to scale the amplitudes of the far traces to account for the difference in shot size. The data from SP and EP included traces which were common to both near and far-offset sources, and consequently the scale factors were calculated directly from the amplitude ratios of the common traces. However, the receiver which was to record both shots from MB only recorded one of them, and thus direct determination was impossible. The scale factor was estimated using an amplitude versus distance plot and measuring the amplitude difference between the two trace sets. Figure 2.2 shows the amplitude vs. distance curve for shot MB. The displayed amplitudes are the RMS amplitudes for a two second window beginning at the first arrival on each trace. This method indicated that the near traces for shot point MB should be scaled up by a factor of 2.5 relative to the
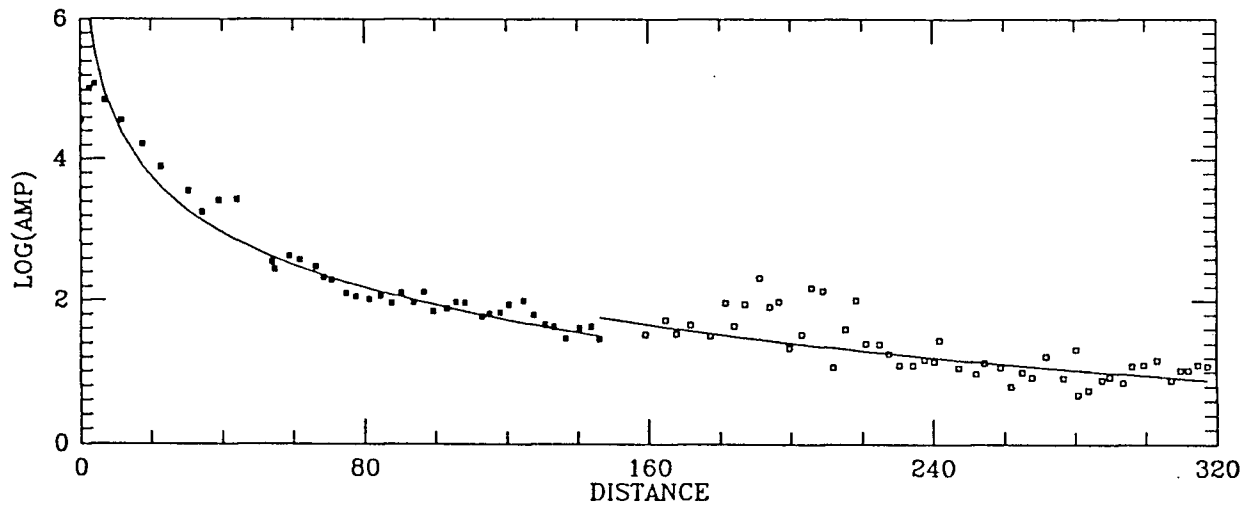
Figure 2.2: Amplitude vs. distance plot for the two shots at MB. Solid squares show the amplitudes of the traces which recorded the smaller shot, while open squares show the amplitudes of those recording the larger shot.

far traces, while shots SP and EP were determined to require scale factors of 2.0 and 1.8 respectively.

Although common maximum amplitude scaling causes arrivals to be visible on all of the traces, it does not permit comparison of the amplitudes of arrivals on different traces and hence is not useful for amplitude modelling. A scale factor proportional to distance raised to the power of 2.4 proved more useful for shots EP and MB while 2.2 was better for shot SP. Figure 2.3 shows the scaling curves which were used. The amplitudes of each trace were divided by the value of the curve at that distance. The triangles show the position of the shotpoints, and the small squares show the RMS amplitudes of a 2 s window starting at the first arrival.

A notable feature of Figure 2.3 is the distinct group of very high amplitude traces between 180 and 220 km. As the same 7 or 8 traces are involved for all three shotpoints, it appears that the high amplitudes are due to near surface effects. The receivers for that part of the line
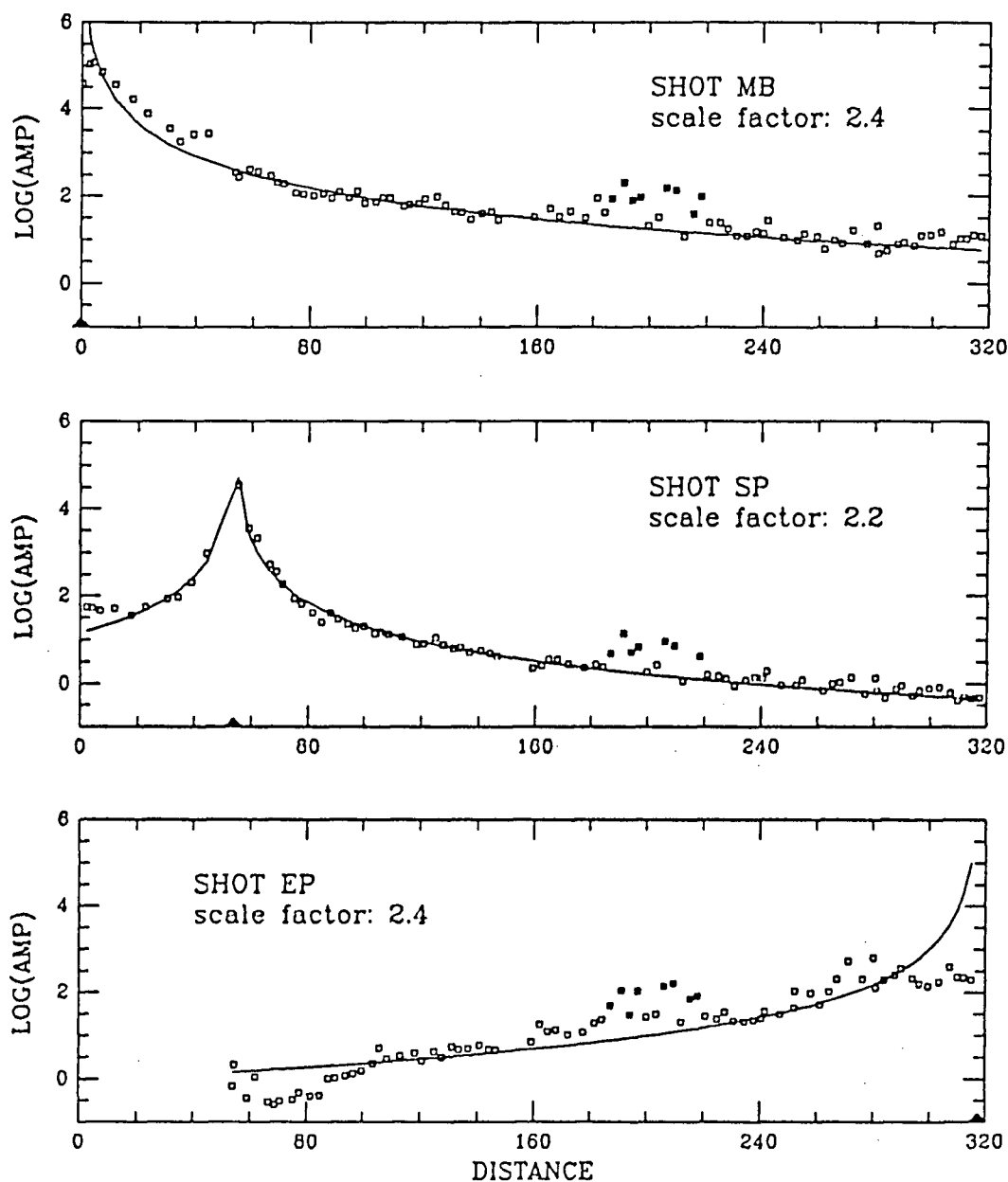
Figure 2.3: Scaled amplitude vs. distance curves. Solid triangles indicate the position of the shotpoint, squares show the RMS amplitudes of the data for each trace, while solid curves show scaling functions – see text for details. Solid squares show traces having anomalous amplitudes.

| Distance | Scale Factors | | | Average |
(km)	EP	SP	MB	Scale Factor
187	0.45	0.45	0.45	0.45
191	0.25	0.25	0.25	0.25
194	0.75	0.45	0.80	0.60
197	0.30	0.40	0.50	0.40
206	0.25	0.30	0.25	0.25
209	0.15	0.40	0.25	0.30
215	0.40	–	0.35	0.40
219	0.40	0.30	0.30	0.35

Table 2.2: Scale factors used to reduce amplitudes in the anomalous zone between 180 and 220 km.

were generally placed on the ice of a frozen river. Lateral changes in the thickness of the unconsolidated sediments directly beneath the receivers and possibly ice characteristics are believed to account for the observed amplitude variations. The modelling of these features is clearly beyond the scope of this experiment. Therefore, the amplitudes of these traces were scaled to a level consistent with the amplitudes of the surrounding traces. For each shotpoint, scale factors were calculated for the anomalous traces by reducing the amplitudes to a value interpolated from the 'good' amplitudes of the adjacent traces. Since the near surface effects at each receiver location should be the same for all shot locations, the three scale factors for each receiver were then averaged so that a common scale factor could be applied to all the traces for that recorder (see table 2.2).

2.3 The Data

All distances mentioned refer to model distances unless otherwise specified.

2.3.1 Shot EP

Shot point EP was located in the Eagle River valley at the southern end of the line. Figure 2.4 shows the data scaled to a common maximum amplitude with the travel-time picks displayed, while Figure 2.5 shows the data scaled by distance to the power of 2.4. A total of 93 traces were recorded.

Fairly clear arrivals can be observed out to a model distance of 60 km (260 km from the shot). The more distant receivers (not shown), which were located on the offshore ice, were extremely noisy. The noise, having amplitudes in excess of 10 times that of the expected seismic signal, was concentrated at frequencies < 5 Hz. Although the signal energy is largely between 5 and 10 Hz at the adjacent onshore receivers, the noise in the signal band at the offshore sites did not allow picks. These traces were therefore muted.

The data exhibit a number of interesting features, the most notable of which are the two zones of very high amplitude arrivals, one between 180 and 220 km and the other between 260 and 300 km. In order to remove near-surface effects, some of the trace amplitudes around 200 km were greatly reduced by selective scaling. The surrounding traces, however, also contained high amplitude arrivals, and consequently an anomalous region remained after the scaling process. It was initially thought that the low amplitudes between these two zones might be due to surface effects such as a layer of loose sediments having a very low Q value (<10) in the region. However, spectral analysis proved inconclusive; there was no substantial difference in the amplitude spectra of the high and low amplitude zones, while a very low Q zone might be expected to cause a substantial reduction of the high frequencies. Subsequent modelling has indicated that this anomaly can be explained by upper crustal structure.

Figure 2.4: Data showing travel time picks for shot EP, reduced using a velocity of 8 km/s and filtered using a trapezoidal bandpass filter (2-4-14-18 Hz). Traces have been scaled to a common maximum amplitude.
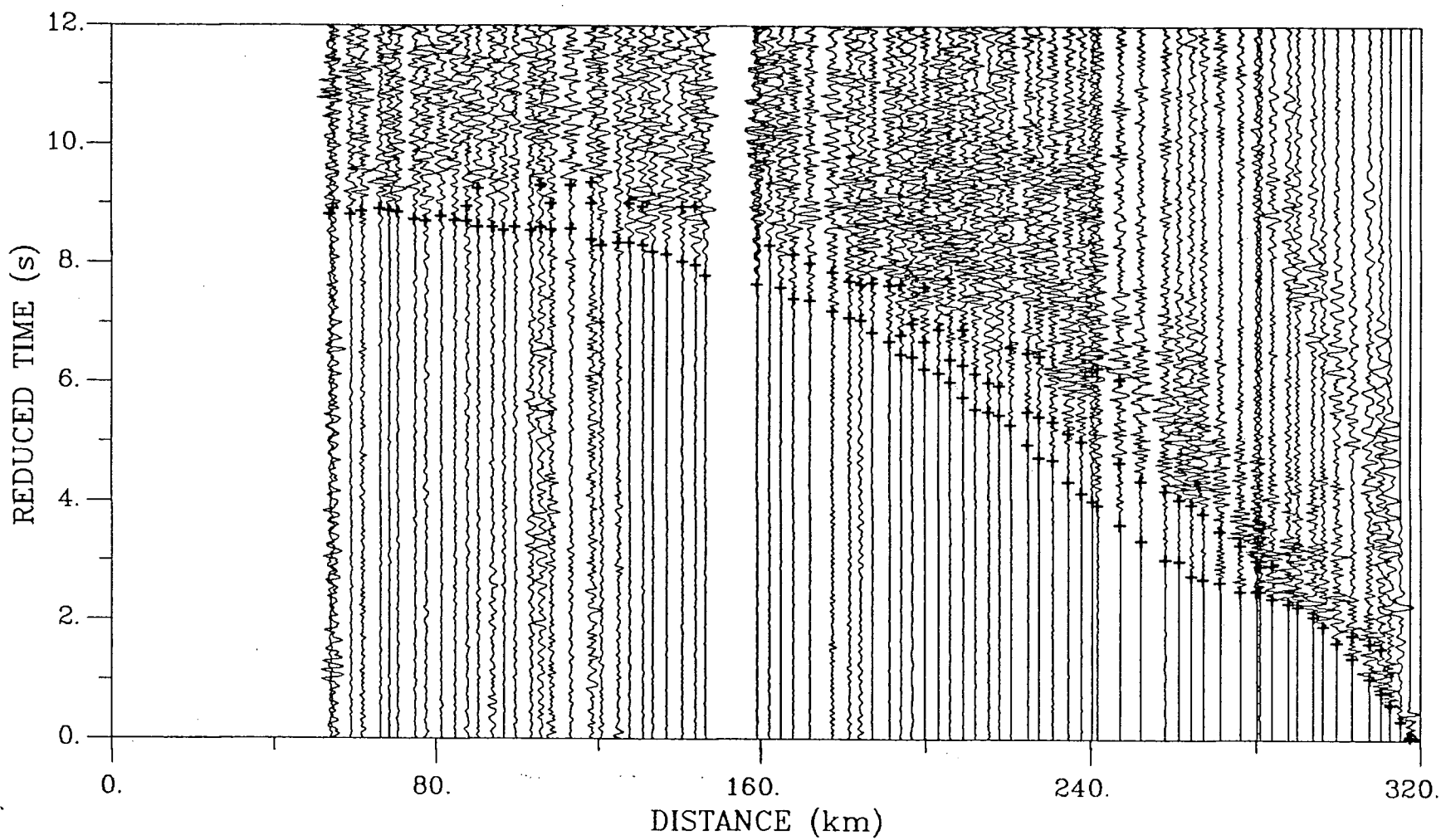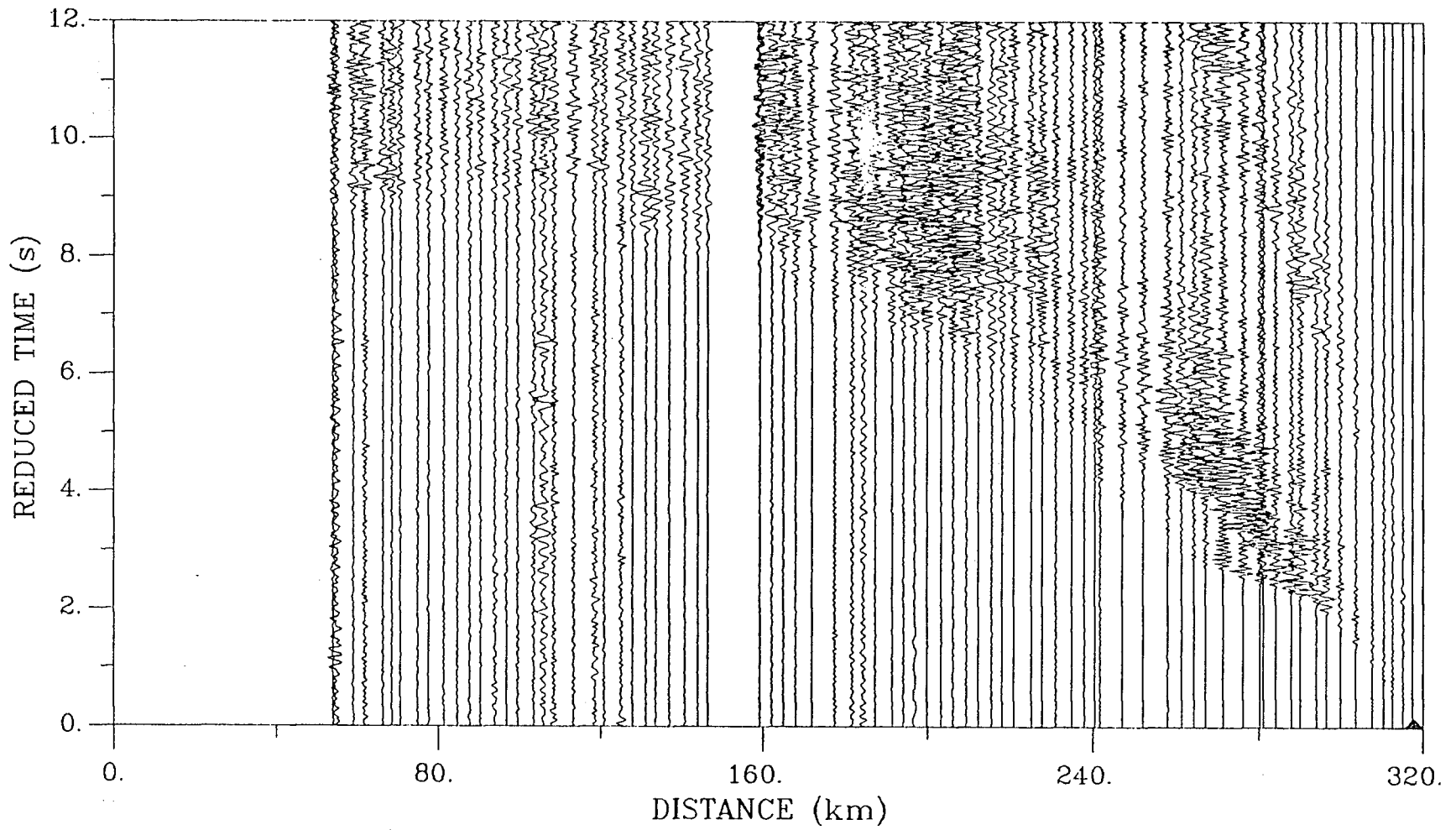
Figure 2.5: Data for shot EP reduced using a velocity of 8 km/s and filtered using a trapezoidal bandpass filter (2-4-14-18 Hz). Traces have been scaled by distance raised to the power of 2.4, while anomalous amplitudes have been scaled down in the 180-220 zone — see text for details.

Another feature is a high amplitude first arrival between 270 and 300 km at approximately 3 s, which has an apparent velocity of over 7 km/s. Both velocity and amplitude are greatly reduced beyond 270 km, with the secondary event having a greater amplitude than the primary between 200 and 270 km. This has been interpreted as being due to a high velocity zone at the base of the sedimentary sequence overlying the lower velocity crystalline basement, combined with a thinning of the sediment layer away from the shotpoint.

There are several other secondary and even tertiary events between 160 and 240 km. They are generally low amplitude and have been interpreted as reflections from midcrustal boundaries. The events between 60 and 180 km, which are interpreted as lower crustal and upper mantle refractions are also very low amplitude, indicating that the velocity gradients are low.

A final point is the presence of very clear shear wave arrivals (Figure 2.6). Since most of the signal energy is in the 1-6 Hz band, its amplitude spectrum is very similar to that of the low frequency noise and cannot be satisfactorily separated by frequency filtering. Although the high amplitude of the signal allowed the picking of many arrivals, the associated errors may be as high as 200 ms. Figure 2.6 is plotted with a reducing velocity of 4.62 and the time axis compressed by $\sqrt{3}$ compared to Figure 2.4. As a result, for a Poisson's ratio of 0.25 throughout the crust, the two plots should be similar. A comparison reveals that shear wave arrivals from the sedimentary layers are as much as 1 s late, suggesting a high Poisson's ratio, while arrivals from the upper crust are somewhat fast, suggesting a low Poisson's ratio. However, the lower crustal arrivals are comparable and indicate that Poisson's ratio averaged over the entire ray paths is close to 0.25.
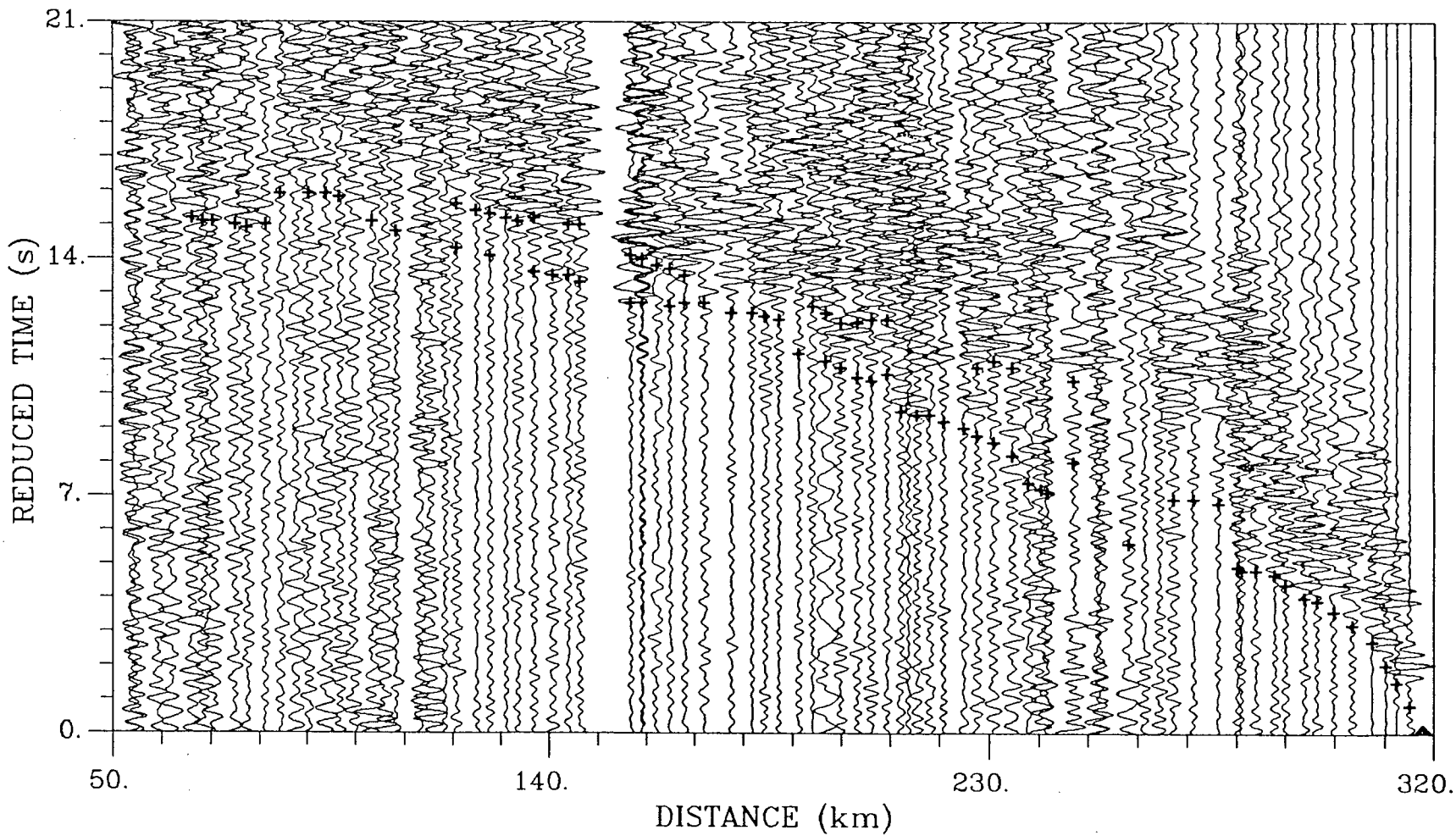
Figure 2.6: Shear data for shot EP reduced using a velocity of 4.62 km/s and filtered using a trapezoidal bandpass filter (0-1-3-4 Hz). Traces are scaled to a common maximum amplitude.

2.3.2 Shot SP

Shot point SP was located near Shingle Point on the shore of the Beaufort Sea. Figure 2.7 shows the data scaled to a common maximum amplitude with the travel-time picks displayed, while Figure 2.8 shows the data scaled by distance raised to the power of 2.2. Only 91 traces were recorded, 10 from receivers on the ice to the north and 81 from the land based receivers to the south.

This data set is very similar in character to that of shot point EP, with the frequency of the signal ranging up to 15 Hz, but with most of the energy being contained in the frequency band between 5 and 10 Hz. The high amplitude zone between 180 and 220 km is clearly evident, and, as for EP, the receivers on the ice were very noisy. However, because the shotpoint here is nearby, the high amplitudes on the near traces enabled accurate first arrival picking of the closest 5 traces, with errors less than 50 ms. Bandpass filtering made it possible to see arrivals on the other northern traces, but picking errors were much higher, likely at least 100 ms.

The first arrivals to about 200 km south of the shot, interpreted as upper crustal in origin, are high amplitude and could be easily picked. However, at greater distances the arrivals are much lower amplitude and thus have much less accurate picks. Their low amplitudes agree with the observations from shot EP that velocity gradients must be low in the lower crust and mantle.

Strong secondary arrivals are present, particularly between 120 and 160 km at a reduced travel-time of approximately 5 s as well as between 180 and 220 km at about 7 s. These have been interpreted as reflections off an upper crustal reflector and the Moho respectively. Shear arrivals are also present (Figure 2.9), however the signal-to-noise ratio is so low on most traces that picking was difficult, with errors up to 200 ms. High amplitude near-source arrivals agree with the previous observation that Poisson's ratio is high in the sediments and

Figure 2.7: Data showing travel-time picks for shot SP, reduced and filtered in the same manner as Figure 2.4, with traces scaled to a common maximum amplitude.

Figure 2.8: Data for shot SP reduced and filtered in the same manner as before. Traces have been scaled by distance raised to the power of 2.2, while anomalous amplitudes have been scaled down in the 180-220 zone – see text for details.

Figure 2.9: Shear data for shot SP reduced using a velocity of 4.62 km/s and filtered using a trapezoidal bandpass filter (0-1-3-4 Hz). Traces are scaled to a common maximum amplitude.

low in the upper crust, while Moho reflections indicate that the average Poisson's ratio for the crust is about 0.25, as was observed at EP.

2.3.3 Shot MB

Shot point MB was located at the northern end of the line, approximately 50 km offshore in Mackenzie Bay. A total of 94 traces were recorded, the nearest 11 from receivers on the ice and the remainder from receivers on land. For this shot, the charges were loaded through the ice onto the sea floor, and as a result, the character of the signal is very different than that from EP and SP, where drill holes were used. The signal does not contain frequencies greater than 10 Hz, while most of the energy is concentrated in the frequency band between 2 and 7 Hz. Figure 2.10 shows the data scaled to a common maximum amplitude with the travel-time picks displayed, while Figure 2.11 shows the data scaled by distance raised to the power of 2.4. Shear arrivals were not observed.

The data quality is much higher for this shot than for the other two; the signal-to-noise ratios on most traces is significantly greater than 2, even for the very low amplitude events from the lower crust and upper mantle. The offshore receivers were remarkably noise free, indicating that the source coupling was much better than for SP. A high amplitude water event is clearly observable on all of these traces with an indicated velocity of 1.40 km/s, as expected for sea water at a temperature near 0° C.

Several interesting features are present. Two very distinctive deflections in the travel-time curves of the first arrival events indicate structural complexity. The sharp slope increase at approximately 80 km corresponds to the edge of the Beaufort-Mackenzie Basin, while the early arrivals near 160 km correspond to the location of the Aklavik Arch. Several strong secondary events are also present. In particular, the event at approximately 100 km, which is picked at a reduced time of about 9 s, is interpreted as a reflection from the Moho, while
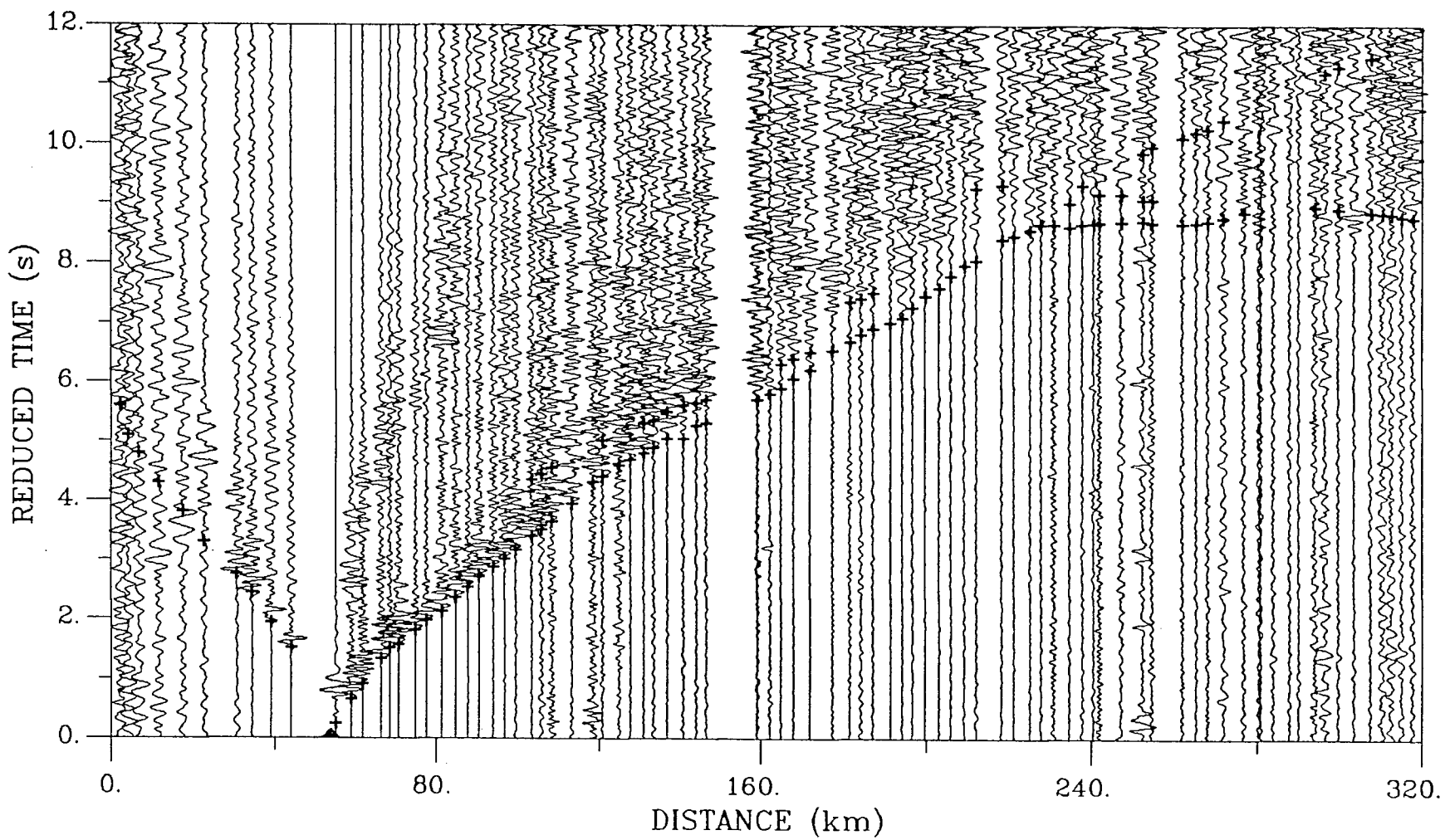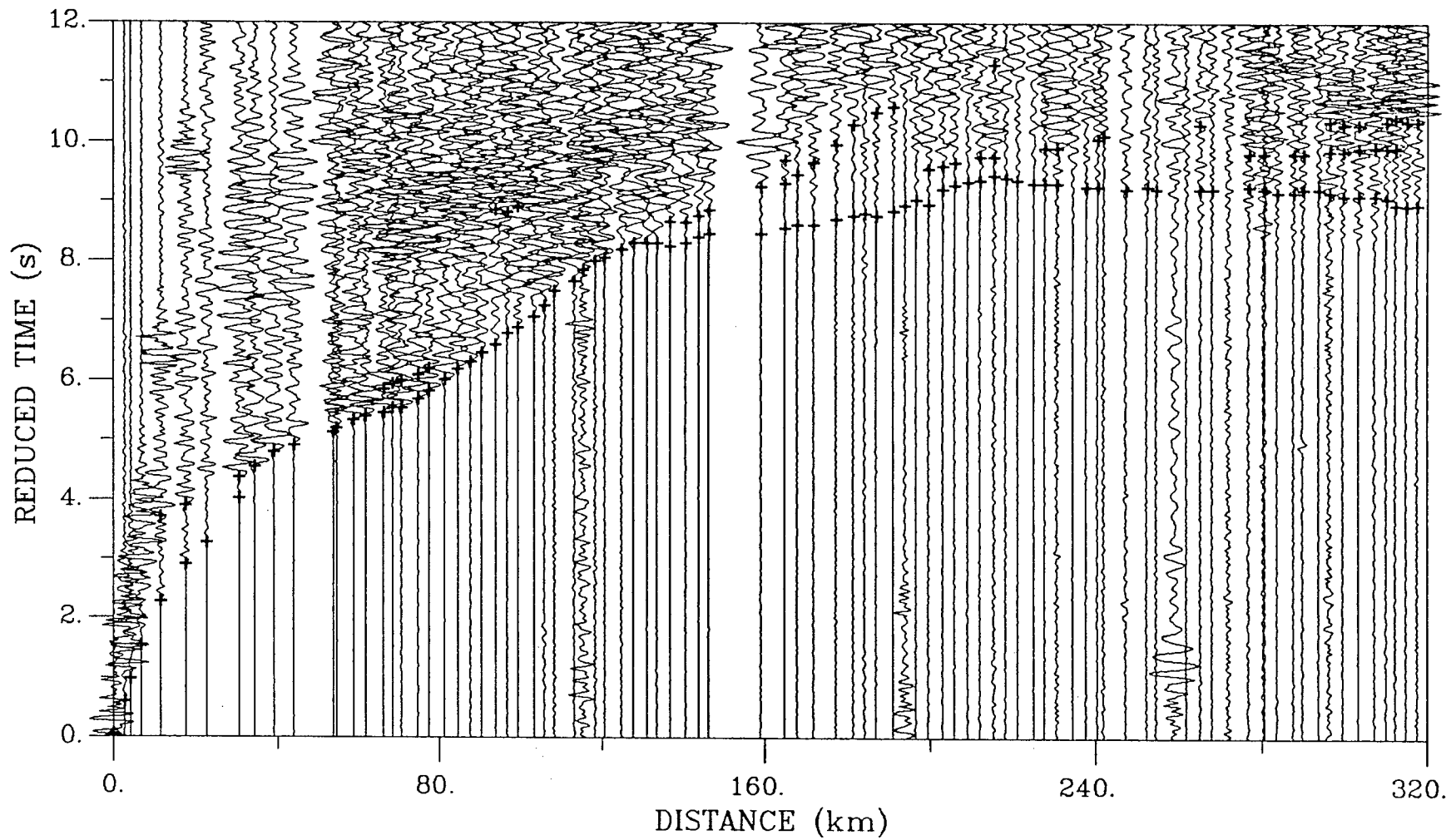
Figure 2.10: Data showing travel-time picks for shot MB, reduced and filtered in the same manner as Figure 2.4, with traces scaled to a common maximum amplitude.
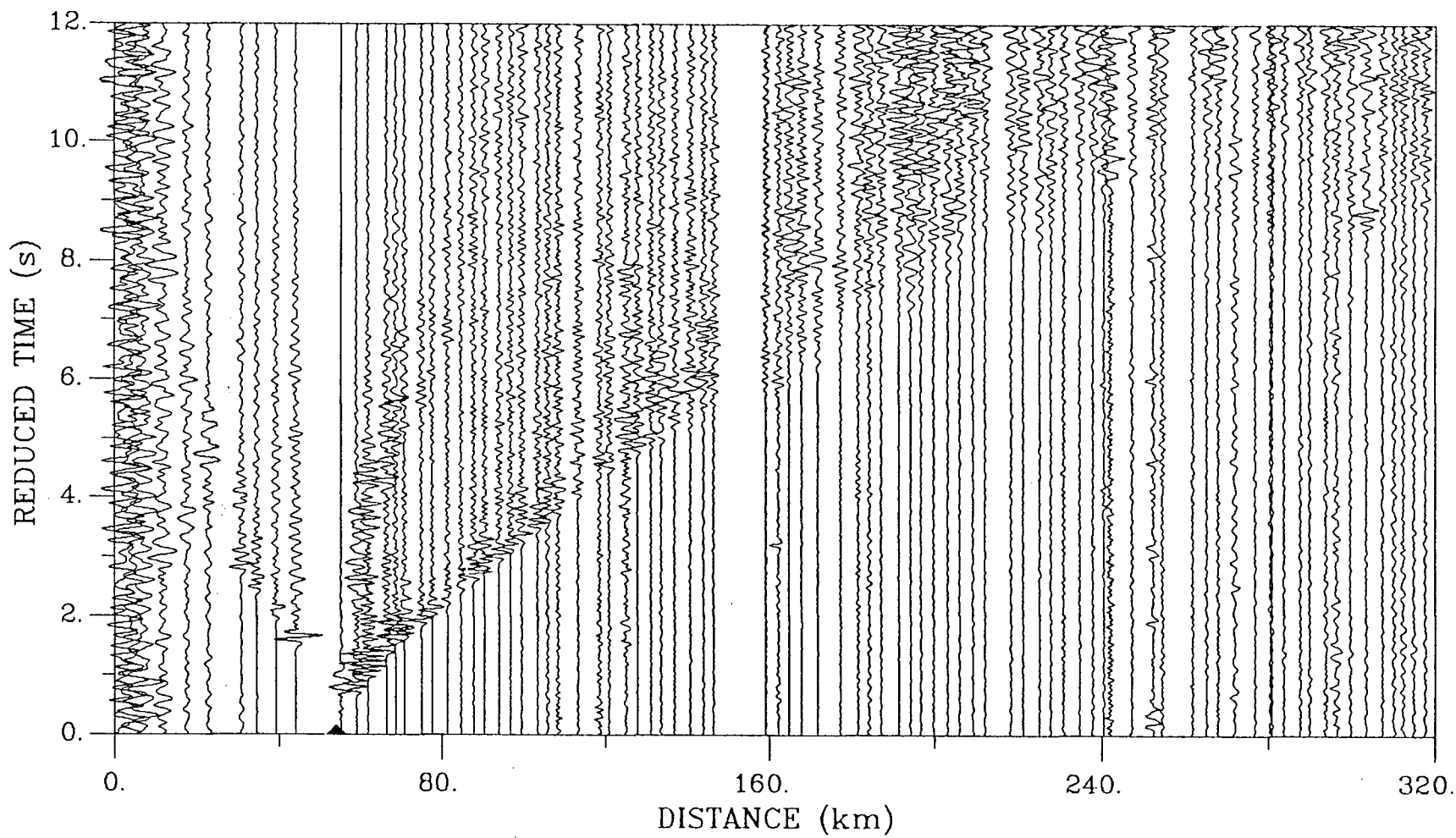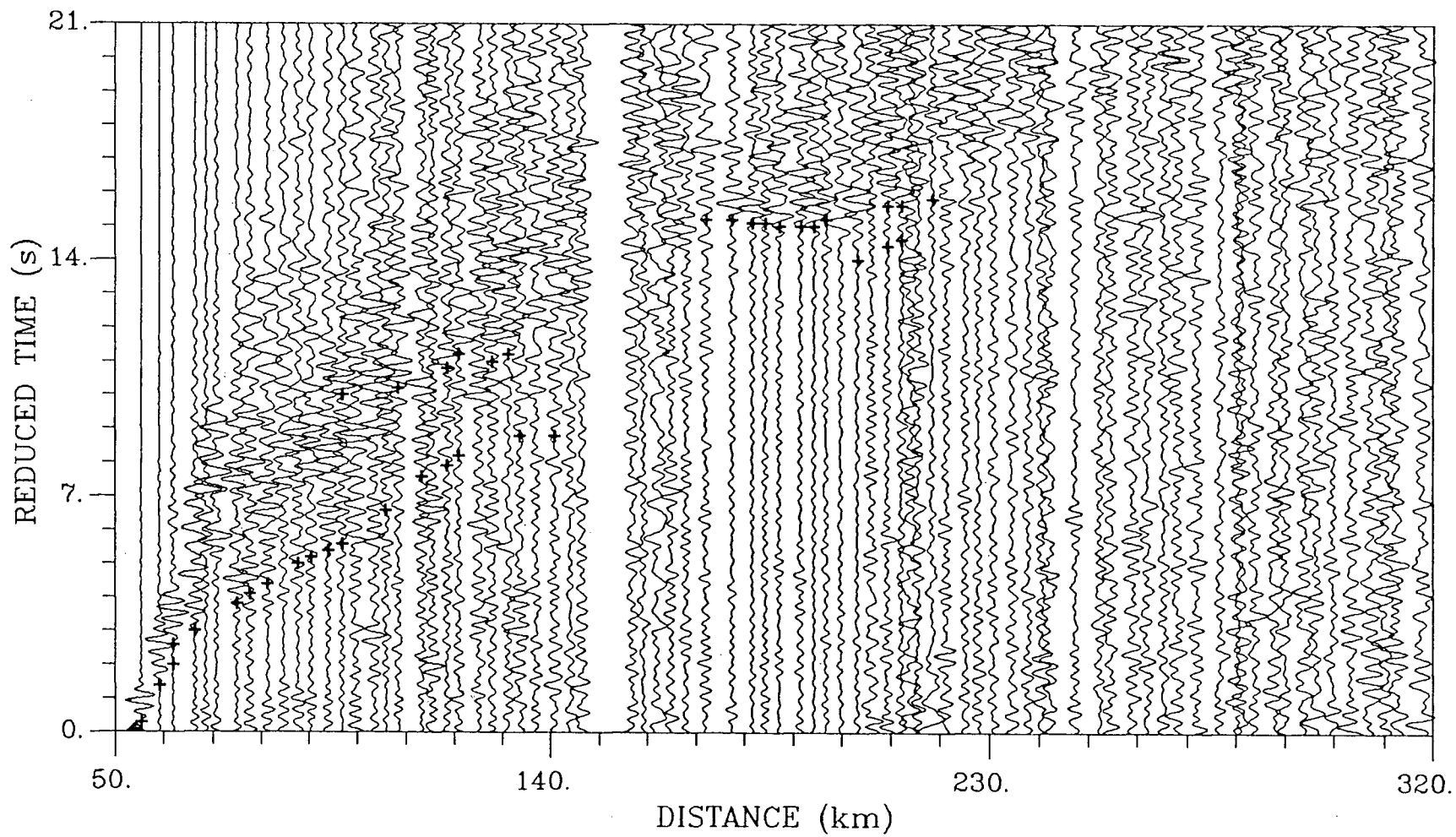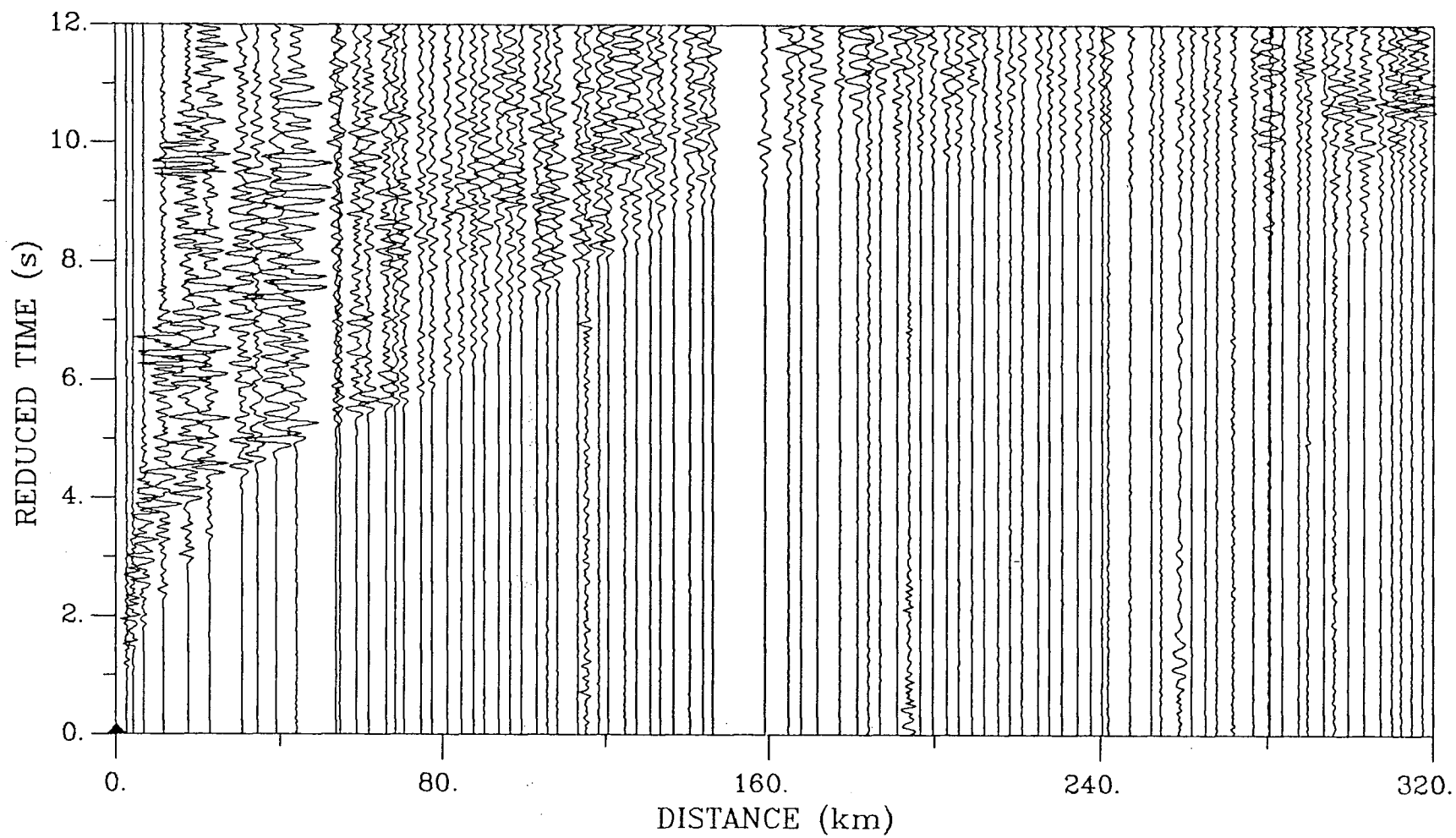
Figure 2.11: Data for shot MB reduced and filtered in the same manner as before. Traces have been scaled by distance raised to the power of 2.4, while anomalous amplitudes have been scaled down in the 180-220 zone – see text for details.

the event at about 10.5 s between 300 and 320 km is interpreted to be wide angle reflections from the same boundary. The lack of high amplitude arrivals between these picks indicates that the Moho is not a uniform boundary. The data agree with the previous observations that crustal and upper mantle velocity gradients are low.

Chapter 3

ANALYSIS

3.1 Introduction

The structural modelling of the data for this experiment is a severely underdetermined problem due to the wide spacing of receivers and the lack of intermediate shots. As a result, secondary arrivals, wherever they could be reliably picked, were used to complement the primary arrivals, and amplitudes were modelled in addition to the travel-times. To provide additional constraint, surface geological observations were incorporated into the model, and information from several sonic logs were used to constrain sediment velocities in the Beaufort-Mackenzie Basin. However, no other geophysical data were available to add reliable constraints to the deep crustal structure.

Several guidelines were followed in order to construct a 'realistic' model. Because of the wide shot and receiver spacings, it was only possible to model broad scale features, and hence, every effort was made to keep the model simple and to include only those layers which could be clearly justified. A layered structure was used, having velocities generally increasing from the surface down. Although the layers were permitted to vary in thickness across the section, lateral velocity variations within the layers were kept to a minimum, with discontinuities limited to 0.05 km/s. Finally, since the modelling was performed using an ART algorithm, the layer boundaries were modelled to be as smooth as possible, in order to eliminate the problems associated with sharp corners.

3.2 The *RAYHASH* algorithm

The travel-times and amplitudes were modelled using RAYHASH, a ray tracing algorithm developed by Zelt and Ellis (1988) based on zero-order asymptotic ray theory (Červený et al., 1977). The algorithm includes approximations which allow the calculation of head wave amplitudes and the amplitude effects of finite Q. The model is defined in terms of trapezoidal blocks which have constant velocities on both top and bottom faces with a linear velocity gradient between. Densities were determined using the expression (Birch, 1964):

$$\rho = 0.252 + 0.3788\, v_p.$$

There are a number of limitations with zero-order asymptotic ray theory. It is inaccurate or invalid near caustics and critical points, as well as in the transition zone between areas of high and low amplitude arrivals (Zelt and Ellis, 1989). Because it assumes an infinite frequency signal, wave effects such as diffractions and multiple scattering may cause substantial inaccuracies in geologically complex regions (Cormier and Spudich, 1984). However, the efficiency of calculations and the ease of use of ART based algorithms easily compensate for the lack of accuracy in certain situations. As a result, asymptotic ray theory provides a very effective method for the forward modelling of seismic refraction data.

3.3 P-wave Data

3.3.1 Modelling procedure

To account for the curvature of the earth, the upper surface of the model was defined by an arc, upon which a simplified topography was superimposed. Layers were approximated by series of trapezoidal blocks having similar velocities and gradients.

The starting point in refraction modelling is often a 1D travel-time inversion to obtain a simple layered velocity structure. However, because of the structural complexity of the

sediments in this study area, this approach was not appropriate. Instead, an initial model was constructed for the sedimentary sequence using the available geological information. In the Beaufort-Mackenzie Basin and the Rapid Depression, estimates of near-surface velocities derived from several sonic logs (Peach, 1988) were used, while the travel-time curves for shotpoints MB and SP were used to estimate deeper velocities. The total sedimentary thickness was initially set to a maximum of 12 km in the Beaufort-Mackenzie Basin and 4 km in the Rapid Depression, in accordance with the predictions of Dixon et al. (1985). For the rest of the line, a map of regional geology (Norris, 1984) was used to locate the surface expressions of major boundaries, including the edges of the White and Rat Uplifts and the location of the Deception Fault. The sedimentary sequence beneath the uplifts was thinned to 2 km. Between the Rat Uplift and the Deception Fault, the sediment thickness was initially set to 4 km, with the same velocities as those in Rapid Depression. A vertical boundary was placed at location of the Deception Fault as geological information indicates that the fault is near vertical at the surface. Starting estimates for sedimentary layer thicknesses and velocities in the Richardson Anticlinorium were obtained from the slope and intercepts of the travel-time curves of the data from shotpoint EP.

Once a starting model was constructed, RAYHASH was used to calculate travel-times through the sediment layers in the Beaufort-Mackenzie Basin for shots at SP and MB, and the model was subsequently adjusted until there was reasonable agreement (generally within 0.10 s) with the observed arrivals. The sediments of the Richardson Anticlinorium were then modelled in the same manner using the data for shotpoint EP. Refractions and head wave arrivals from the base of the sedimentary sequence between SP and the Deception Fault allowed the thicknesses to be estimated, assuming the initial velocities were correct.

When the sediments fit the travel-time data satisfactorily, the deeper structures were modelled. Since reflection and refraction studies from elsewhere have generally indicated that the crust consists of at least two distinct layers, a simple two layered crystalline crust,

having velocities and thicknesses which were calculated from the arrival time versus offset curves for the picks from the three shots, was initially modelled here. Again, travel-times were calculated using RAYHASH, and the model was adjusted until reasonable fits (0.10 – 0.15 s) to the data were obtained.

Once the travel-time fit was acceptable, the amplitudes were modelled. The velocity gradients within the layers were adjusted to generate better matching refracted amplitudes, while the magnitudes of the velocity discontinuities between layers were adjusted to obtain better fitting reflected amplitudes. Since this inevitably caused a misfit in the travel-times, the layer thicknesses then had to be adjusted until the time fit was improved.

After several iterations, a model was obtained which fit both the travel-times and amplitudes. First arrival picks were generally fitted to within 0.05 seconds, while the secondary arrivals and the less accurate of the primaries were fitted to within the best estimate of their errors. Since amplitudes can be influenced by near-surface structures which are beyond the resolution of this type of survey, only broad scale amplitude trends were modelled. Also, because reflection amplitudes are particularly dependent on fine scale structures (Christensen and Szymanski, 1988), matching the reflected amplitudes was given a lower priority than matching refractions.

3.3.2 The model

The final model may be divided into five main layers, as shown in figure 3.1. Figure 3.2 shows how velocity varies with depth at model distances of 40 km, 120 km and 300 km. The sediments, having velocities ranging from 2.0 to 5.5 km/s in the Beaufort-Mackenzie Basin in the north, and 4.2 to 6.35 km/s in the sediments of the Richardson Anticlinorium in the south form the upper layer. A 30 metre thick water layer (velocity: 1.4 km/s) at the surface of the northern 45 km of the line and a 100 m thick (Mackay, 1967) permafrost layer
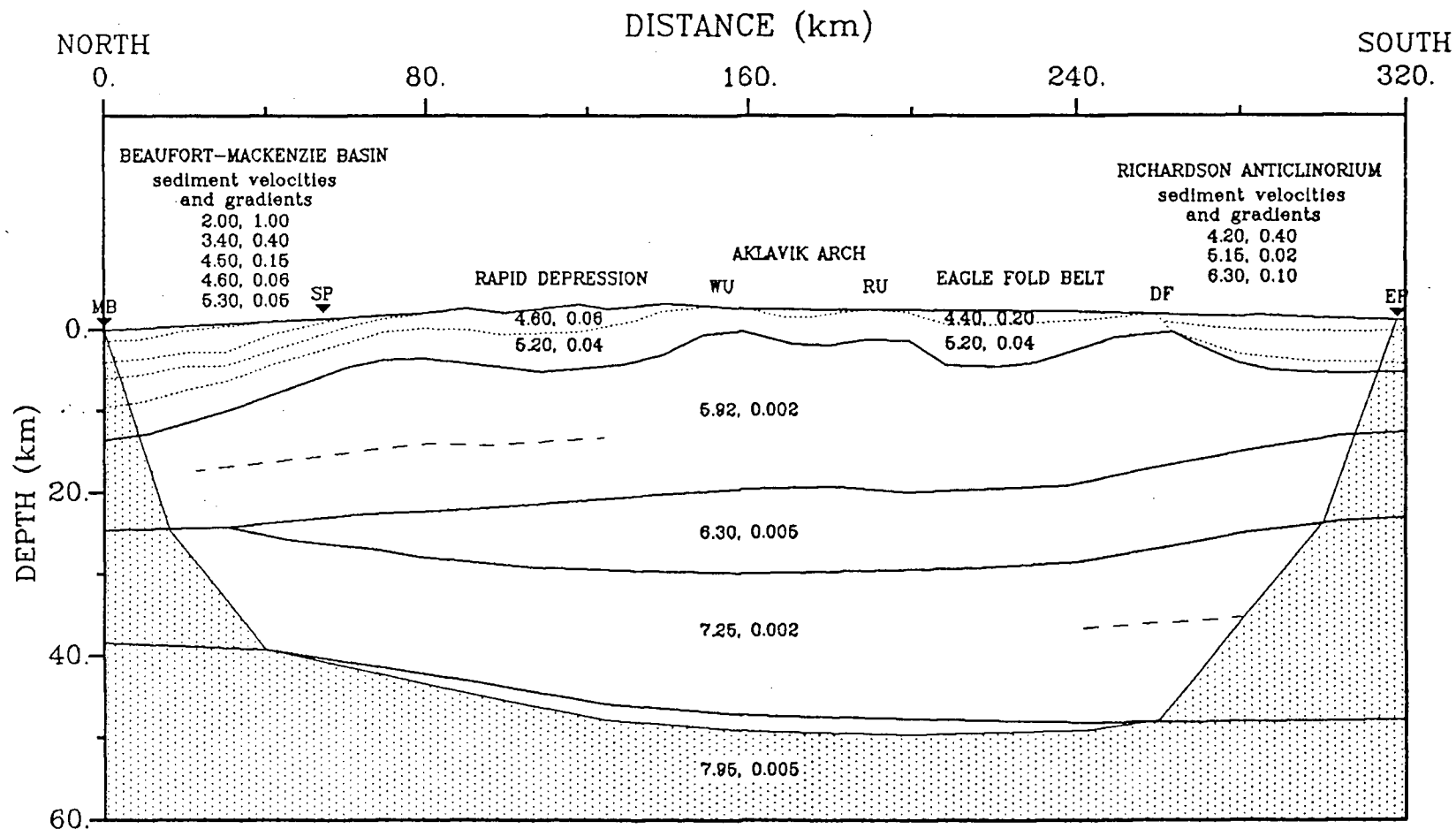
Figure 3.1: The P-wave model. Numbers refer to the velocities (km/s) at the top of each layer as well as the layer's velocity gradient (s⁻¹). Solid lines show layer boundaries, dotted lines show sedimentary boundaries, and dashed lines show internal reflectors. Shaded areas are beyond the limits of the ray coverage. (WU–White Uplift, RU–Rat Uplift, DF–Deception Fault). See Figure 3.2 for depth profiles at 40, 120 and 300 km.

Figure 3.2: Depth profiles showing the P-wave velocities of the model a) at 40 km (Beaufort-Mackenzie Basin), b) at 120 km (Rapid Depression) and c) at 300 km (Richardson Anticlinorium).

(velocity: 3.5 km/s) which covers the southern 50 km are not shown, but were included in the calculations. Beneath shotpoint MB, the sonic logs from the wells, Adlartok P-09 (15 km to the northw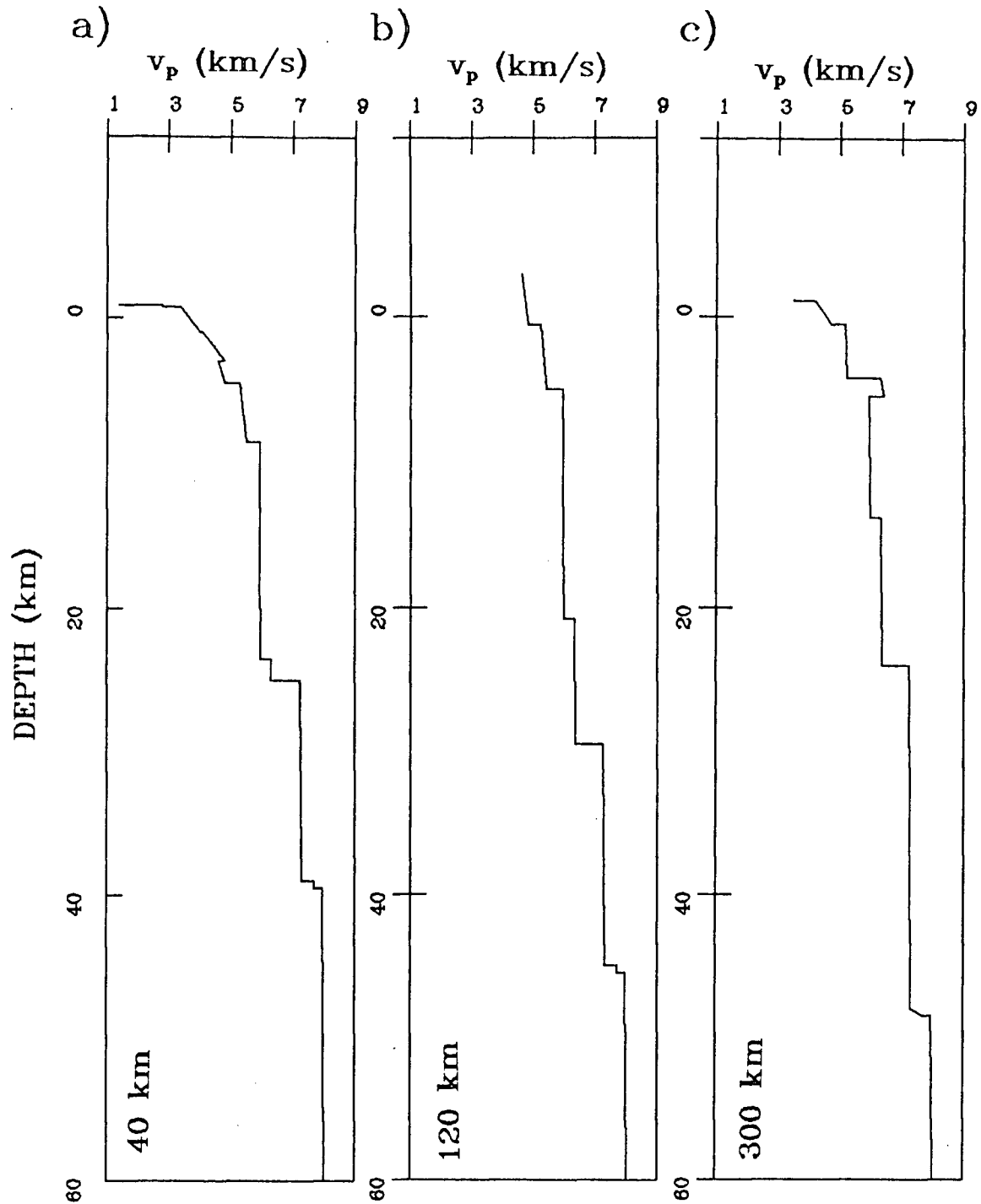est of MB) and Sarpik B-35 (23 km to the east of MB) were used. These had velocities which increased from about 2 km/s to 4 km/s in the top 3 km of sediments. Beneath shotpoint SP, two other wells, Fish River B-60 (30 km east of SP) and Blow River E-47 (6 km southwest of SP), which had velocities over 3 km/s near the surface increasing to 5 km/s by a depth of 3 km, were used.

Immediately below the sediments lies the crystalline upper crust, which has velocities ranging from 5.92 at its top to 5.96 km/s at its base. A midcrustal layer with velocities from 6.3 to 6.35 km/s, is also present. Although it has a thickness near 10 km over the southern half of the line, it pinches out beneath the edge of the Beaufort-Mackenzie Basin. The lower crustal layer, having an upper velocity of 7.25 with a low gradient of 0.002 km/s, also thins toward the north, from a thickness of 24 km in the south to only 14 km beneath shot MB. Both the upper and lower crustal layers contained intermediate reflectors. The crust thins from a maximum thickness of 49 km beneath the Richardson Mountains to 38 km at the northern end of the line. The upper mantle was determined to have a velocity of 7.95 km/s.

For modelling purposes, values for Q in the sediments were obtained from Mitchell and Hwang (1987). The Quaternary sediments near the surface were assigned a value of 50, while the older sediments were given progressively higher Q values to a maximum of 250. The upper and middle crust were assigned values of 500 and 750 respectively, while the lower crust and upper mantle were given values of 1000. These are consistent with the values derived by Zelt and Ellis (1990) for the crust and upper mantle in the Peace River Arch region of northern Alberta.

3.3.3 Shot EP

Figure 3.3 shows rays traced through the model from shot EP, and the calculated and observed travel-times, while Figure 3.4 shows the synthetic and observed seismic sections (see Figure 2.4 for the travel-time picks displayed on a section with traces scaled to a common maximum amplitude). The travel-times for the model fit the data very well. Within 100 km of the shot point, the calculated first arrival times are generally within 0.05 s. Further from the shot, the travel-times do not fit quite so well, but are still within 0.10 s, in accordance with the error predictions discussed in Chapter 2. Secondary arrivals also fit the data very well, as almost all arrivals are within the 0.10 s error.

First arrivals are modelled using six refraction and head wave events. Refractions from within the sediments are the first arrivals out to about 280 km model distance. The high apparent velocity event between 270 km and 300 km is the result of a combination of refractions and slightly slower reflections from within the 6.3 km/s layer at the base of the sediments, with the sudden termination being due to a pinch out of the layer at 260 km, the location of the Deception Fault. The lower amplitude first arrivals from 270 km out to about 180 km are interpreted as head wave arrivals from the top of the high velocity layer which continue along the base of the sediment sequence beyond the Deception Fault. From 180 km out to about 60 km, near the end of the useful data, the first arrivals are interpreted to be head waves from along the base of the mid crustal layer. The low velocity gradient of the lower crust and the structure of its upper boundary cause refractions to be only observed near the critical angle. Between 60 km and 80 km, the primaries are upper mantle refractions.

Seven reflected events are evident. The three earliest are all from within the sediment package, with the latter two contributing to the high amplitude events between 260 and 300 km. The fourth, with relatively clear arrivals occurring from 260 km out to 200 km, is modelled as the reflection from the base of the upper crust. The observed amplitudes

DISTANCE (KM)

Figure 3.3: a) Ray paths through the model from shot EP. The model boundaries are marked with heavier lines.

Figure 3.3: b) Observed travel-times for shot EP (0.1 s high diamonds) with calculated times (lines) for the model shown above.
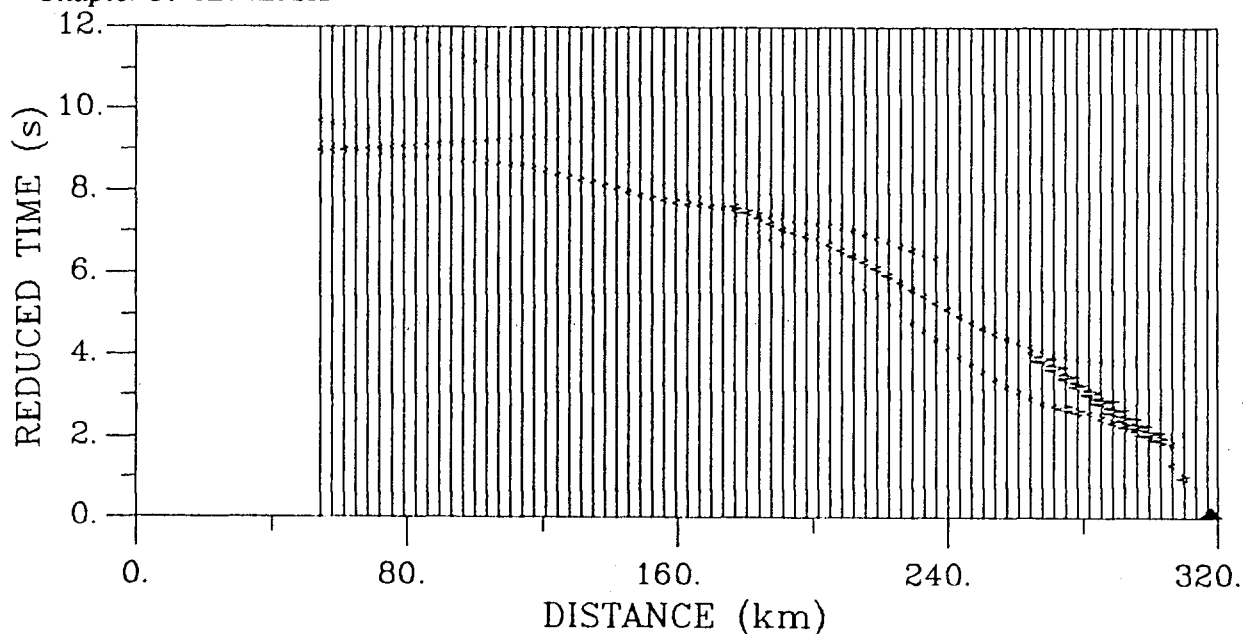
Figure 3.4: a) Synthetic seismograms for shot EP. Since no consistent wavelet could be extracted from the data, a Ricker wavelet (dominant frequency of 10 Hz) was used.
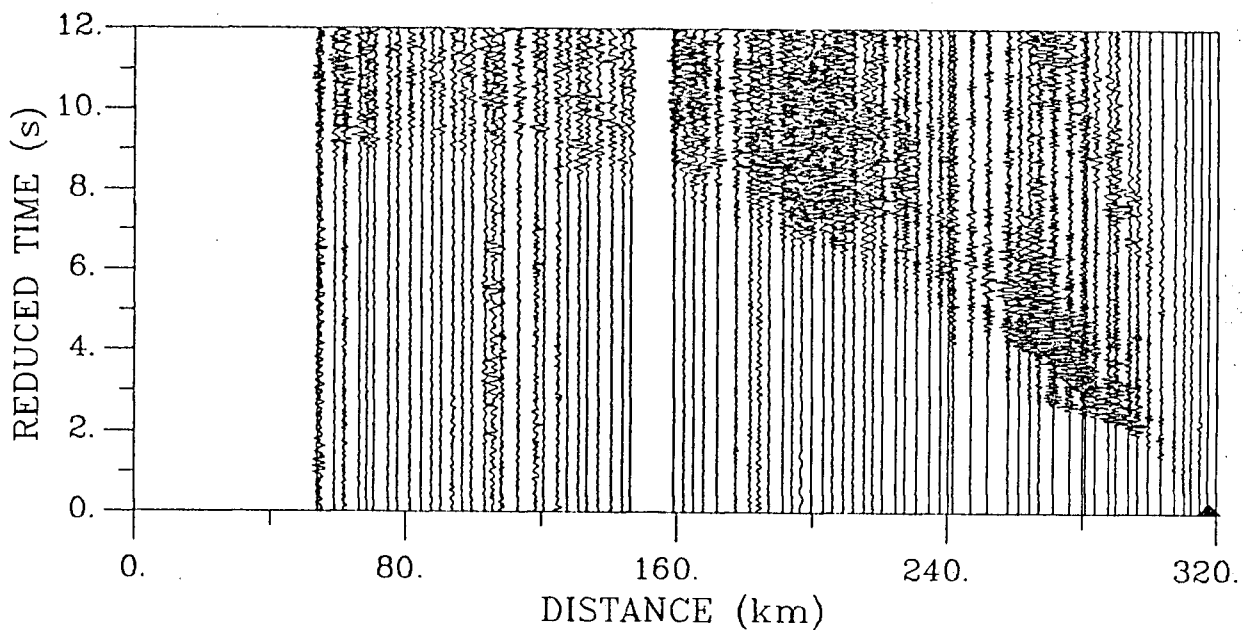
Figure 3.4: b) Actual data for shot EP, bandpass filtered (2-4-14-18 Hz) and scaled by distance to the power 2.4 (see Figure 2.5).

are substantially lower than those expected for a boundary having a 0.34 km/s velocity discontinuity, and as a result the boundary is modelled as a 200 m thick transition zone with a maximum velocity discontinuity of 0.1 km/s. For the fifth reflection event, which has arrivals from 240 km to 200 km at reduced times from 6 to 7 s, the base of the midcrustal layer is modelled in the same manner. The transition zone widths were chosen arbitrarily, since their structure is clearly beyond the resolution of the interpretation procedure, and as a result this may not be representative of the actual boundary geology. The sixth reflection has arrivals between 180 and 200 km and is interpreted as being due to a reflector within the lower crust, located between 240 km and 280 km. The amplitudes for this event were not modelled, as the lower crustal refractions did not indicate a velocity change was required. These reflections are likely caused by internal structures of limited thickness, such as fault zones or intrusions as described by Christensen and Szymanski (1988). The last reflection, at a reduced time of approximately 9 s, was interpreted as being from the Moho. It also has a much lower amplitude than expected for a major 0.65 km/s velocity discontinuity, and consequently the Moho was modelled as a 500 m thick transition zone. Higher amplitudes are observed beyond 80 km, at the northern end of the line, which indicates increased Moho reflectivity between 105 km and 120 km. This was modelled by pinching out the transition zone in that region.

3.3.4 Shot SP

Figure 3.5 shows the rays traced through the model from shot SP and the calculated and observed travel-times, while Figure 3.6 shows the synthetic and observed data (see Figure 2.7 for the travel-time picks displayed on a section with traces scaled to a common maximum amplitude). Again, the travel-time fit is good. To the south of the shotpoint, most of the calculated arrivals are well within 0.05 s, even at the far end of the line. Some of the
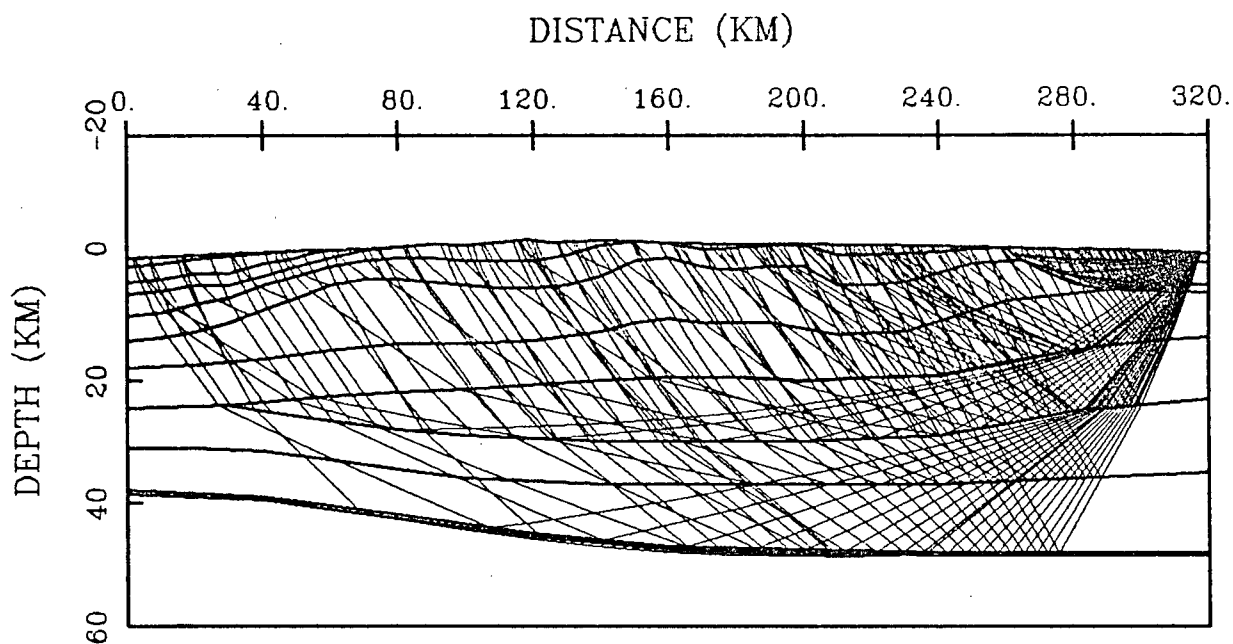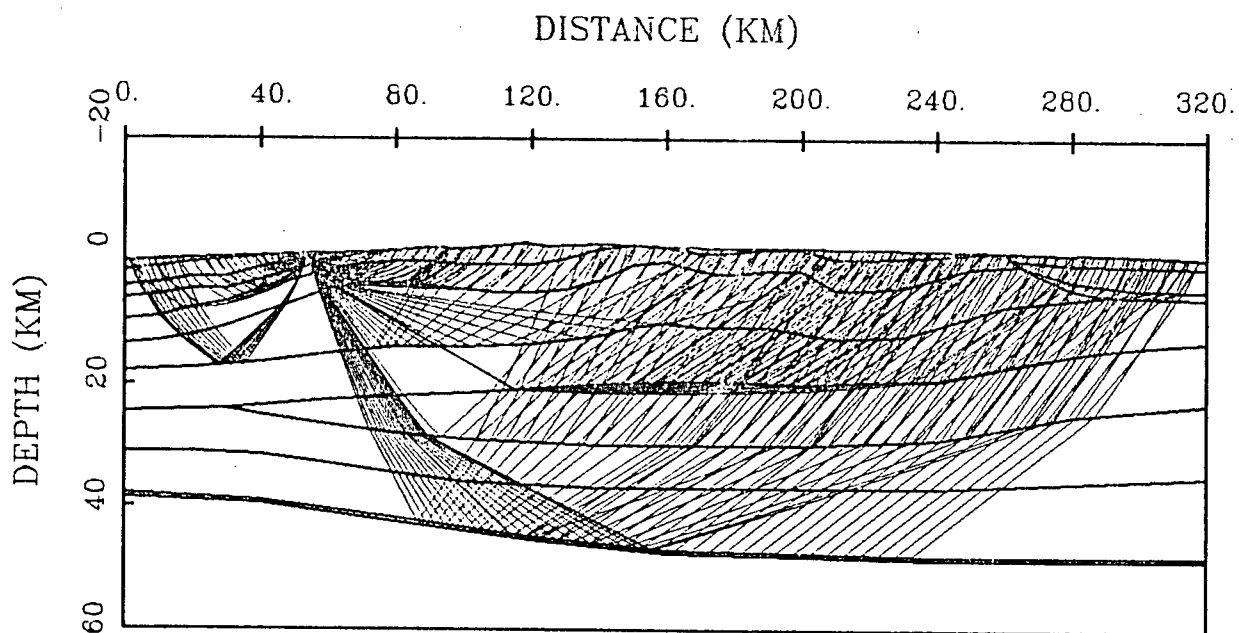
Figure 3.5: a) Ray paths through the model from shot SP. The model boundaries are marked with heavier lines.
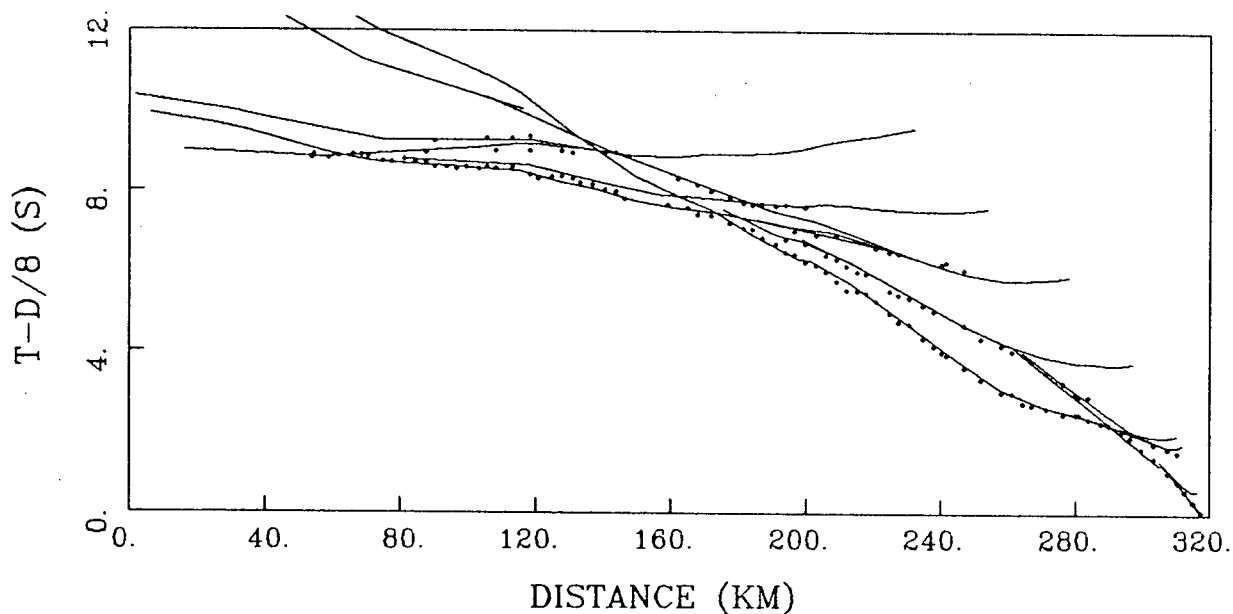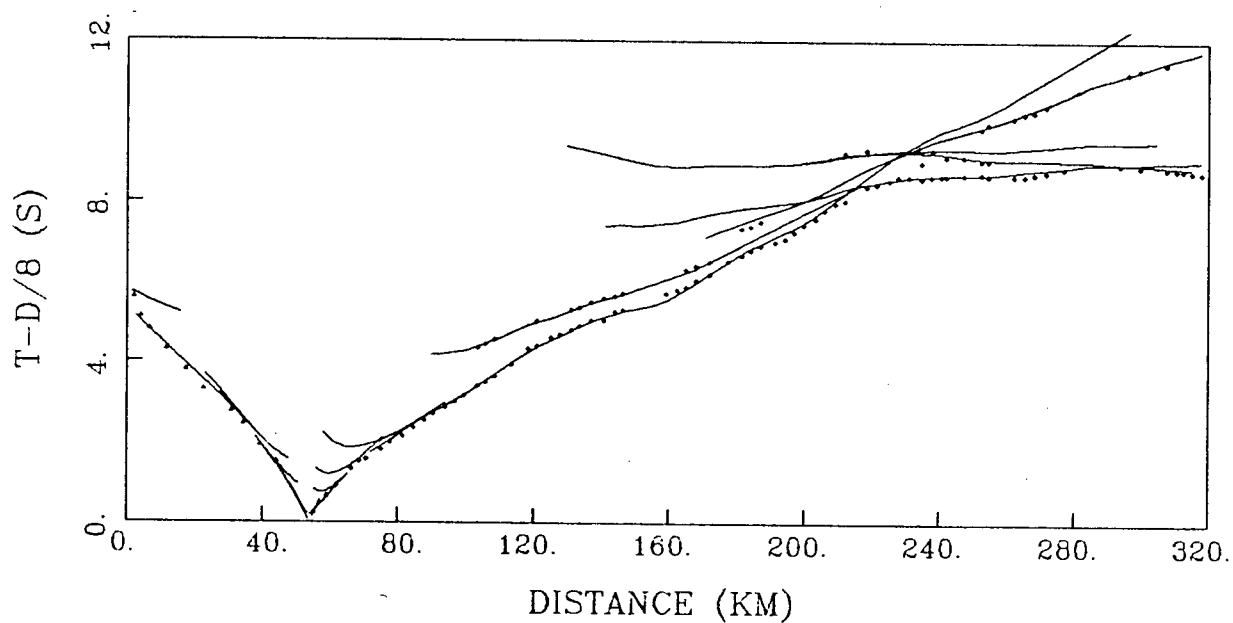

Figure 3.5: b) Observed travel-times for shot SP (0.1 s high diamonds) with calculated times (lines) for the model shown above.
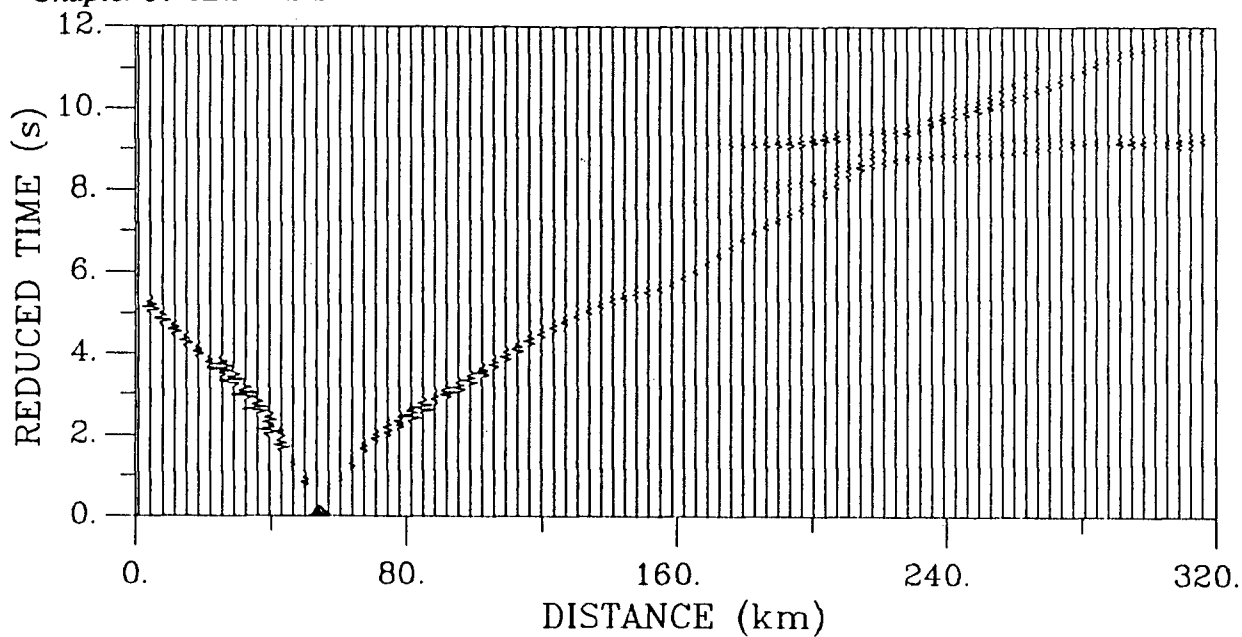
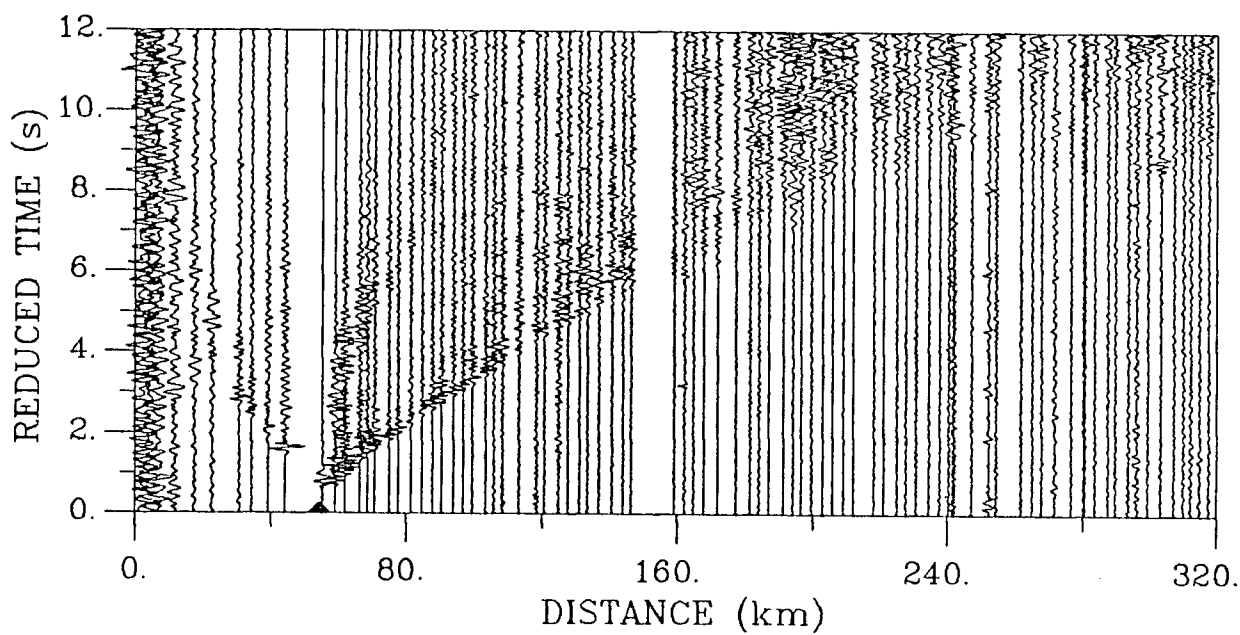Figure 3.6: a) Synthetic seismograms for shot SP. The wavelet was extracted from the data.

Figure 3.6: b) Actual data for shot SP, bandpass filtered (2-4-14-18 Hz) and scaled by distance to the power 2.2 (see Figure 2.8).

secondary picks are not fitted as well, but are still generally within 0.10 s. To the north of the shotpoint, where the data quality deteriorated more rapidly, the travel-time fit is not as good, but most arrivals still match to within 0.10 s.

The first arrivals at the northern receivers are from within the sediments of the Beaufort-Mackenzie Basin. Although most traces are noisy, making it difficult to extract detailed amplitude information, the travel-time observations were adequate to determine the sediment structure. The data do indicate that amplitudes drop off very rapidly at approximately 20 km, and this has been successfully modelled.

The receivers to the south provided better quality data. Detailed modelling of the sediments near the shotpoint, constrained by surface geology and well information, was unable to match the high amplitudes of the near source arrivals. However, near-source arrivals are especially subject to amplitude features which are not modelled by ART, such as reverberations and scattering. Also, amplitudes of events within a sedimentary basin are highly dependent upon small scale sediment structures which are beyond the resolution of this survey. Amplitudes for rays turning beneath the sediment layer are well matched.

First arrivals are modelled by six refraction and head wave events, the first three of which are from within the sediment layers. From 80 km out to almost 220 km the first arrivals are generally modelled as refractions from the upper crust. However, the complex basement structure produced several shadow zones in which head waves were the first arrivals due to the absence of refractions. Two basement highs are modelled near the centre of the line; one near 160 km, which correlates well with the location of the White Uplift, and a smaller one near 190 km, corresponding to the location of the Rat Uplift. The amount of uplift relative to the adjacent basement depths are 4.5 km for the White Uplift and 3 km for the Rat Uplift. From 220 km to 280 km the first arrivals are modelled as head waves along the base of the mid crust. From 280 km to the end of the line the first arrivals are modelled as upper mantle refractions, with head waves from the Moho contributing to the amplitudes. Because the low

amplitudes require a low velocity gradient, the refracted rays turn in the upper one or two km of the mantle and arrive at virtually the same time as the head waves.

Several secondary events are present. The event between 90 km and 180 km was modelled as reflections from within the upper crust. As before, the amplitudes were not modelled, on the assumption that the reflectivity was due to fine scale structure of limited thickness. The secondary arrivals that were picked between 180 km and 190 km, as well as those between 260 km and 300 km at reduced times greater than 10 s were modelled by refractions from within the 6.3 km/s mid crustal layer. Those between 240 and 260 were modelled by upper mantle refractions and head waves from the Moho, while those between 200 km and 240 km were modelled by Moho reflections. The somewhat higher amplitudes near 200 km are from the same reflective zone on the Moho that was seen from shotpoint EP, between 105 km and 120 km.

3.3.5 Shot MB

Figure 3.7 shows the rays traced through the model from shot MB, and the calculated and observed travel-times, while Figure 3.8 shows the synthetic and observed data (see Figure 2.10 for the travel-time picks displayed on a section with traces scaled to a common maximum amplitude). The travel-times fit the data very well. The only first arrivals which are not fit to within 0.05 s are those for the very low amplitude event between 220 and 250 km, which have been estimated to have a picking error of 0.10 s. The secondary arrivals have also been modelled to within 0.10 s.

First arrivals within 50 km of the shotpoint are from sedimentary events in the Beaufort-Mackenzie Basin. The final model includes only those features which could be easily justified from the data. This resulted in a very broad scale sedimentary structure and a very reasonable amplitude fit. The offset in the first arrivals at 30 km has been modelled as a low velocity
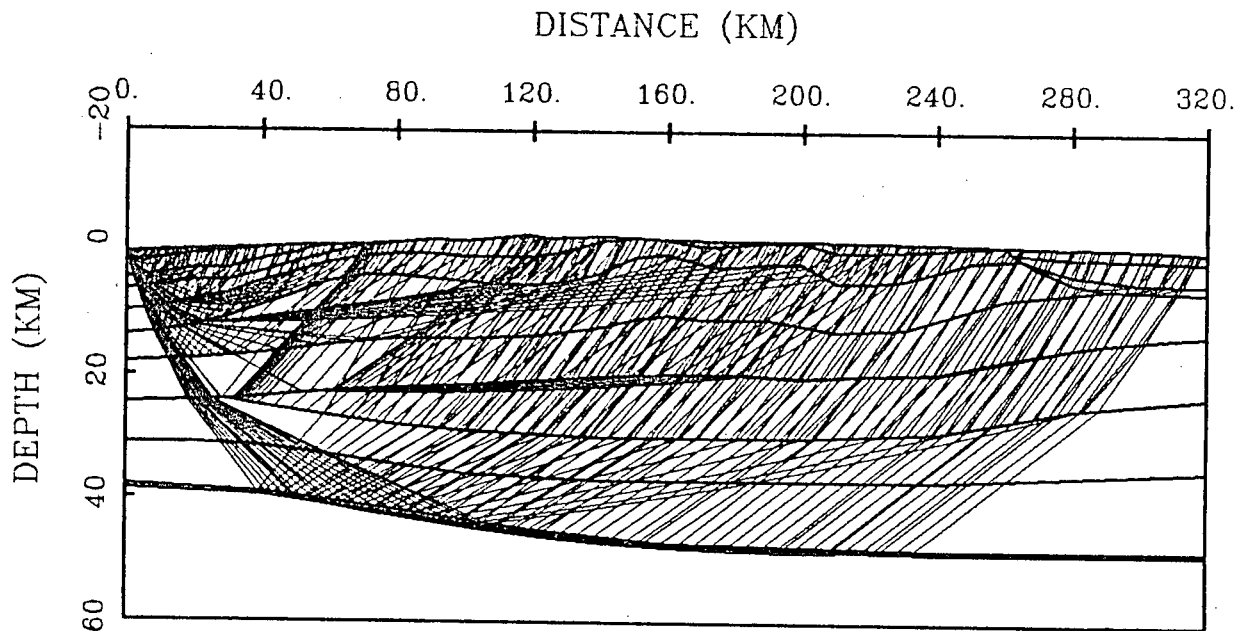
Figure 3.7: a) Ray paths through the model from shot MB. The model boundaries are marked with heavier lines.
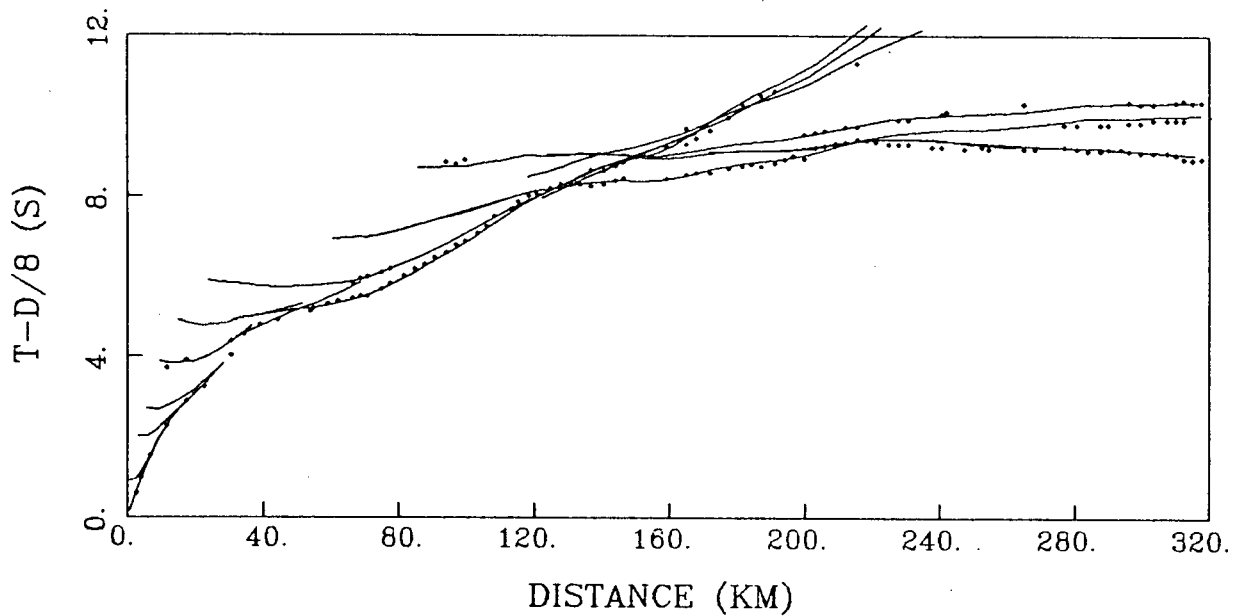
Figure 3.7: b) Observed travel-times for shot MB (0.1 s high diamonds) with calculated times (lines) for the model shown above.
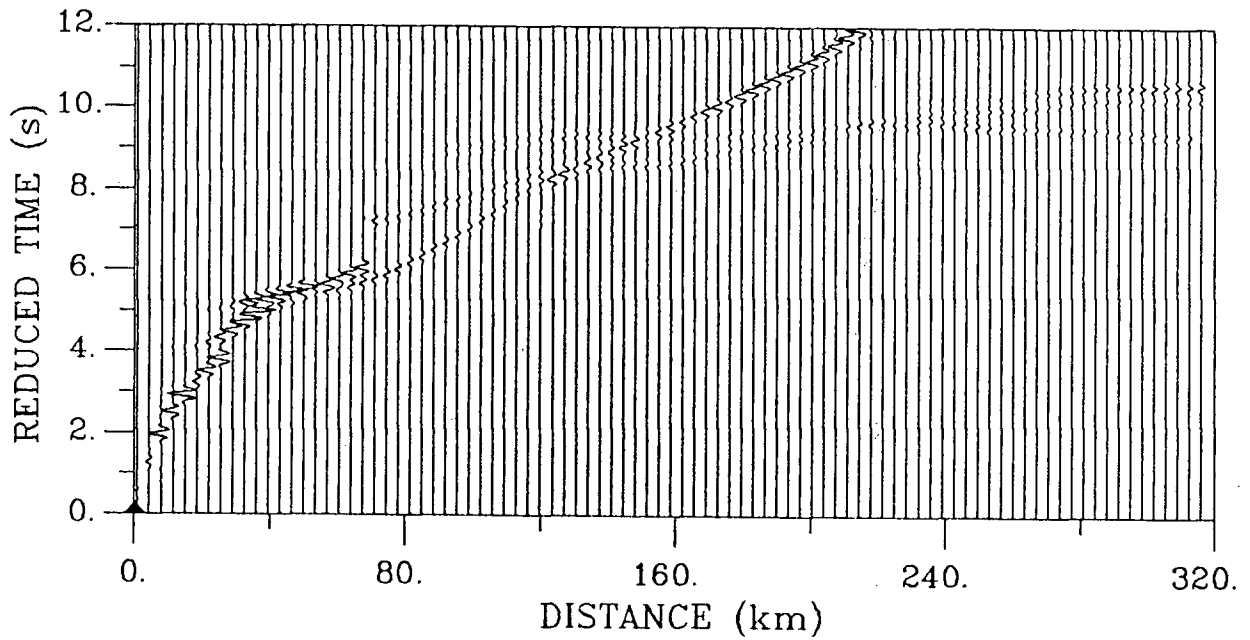
Figure 3.8: a) Synthetic seismograms for shot MB using a Ricker wavelet (dominant frequency 5 Hz).
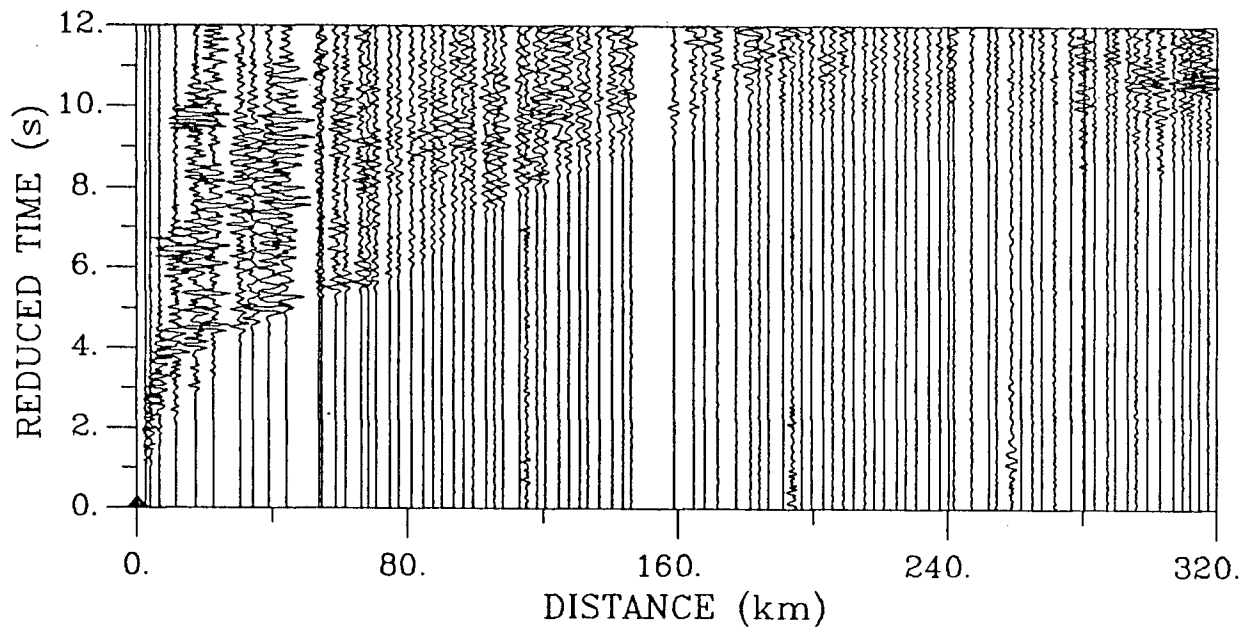
Figure 3.8: b) Actual data for shot MB, bandpass filtered (2-4-14-18 Hz) and scaled by distance to the power 2.4 (see Figure 2.11).

zone at a depth of 6 km below MB (see Figure 3.2), with the velocity at the top of the zone being 0.2 km/s lower than the velocity at the bottom of the overlying layer. The early arrivals in the travel-time curve between 60 and 80 km indicates the presence of a basement high between the Rapid Depression and the main Beaufort-Mackenzie Basin.

The primary arrivals from 50 km to 120 km are produced by refractions from the top of the upper crust, with head waves from the base of the sediments providing arrivals in the shadow zones which result from the complex basement structure. The primary arrivals from 120 km to 220 km are modelled as head waves from the upper boundary of the lower crustal layer, as are the secondary arrivals from 270 km to 310 km. From 220 km to the end of the line, the first arrivals are refractions from the upper mantle, again with head waves contributing to the amplitudes.

Several secondary events have also been modelled. Reflections from a horizon in the upper crust are evident between 60 km and 80 km. The Moho also produced good subcritical reflections between 90 km and 100 km at a reduced time of 9 s and postcritical reflections intermittently between 200 km and the end of the line. The extreme variability of the amplitudes apparently indicates substantial lateral variations in the Moho structure. The high amplitude arrivals near the end of the line have been modelled as wide angle reflections from the same reflective zone which was noted at EP and SP, between 105 km and 120 km, while the arrivals between 90 km and 100 km indicate the presence of another reflective zone, from 40 km to 60 km. As before, these were modelled by pinching out the Moho transition zone in those regions. Refractions from the 6.3 km/s mid crustal layer contribute to the high amplitude secondary arrivals between 160 km and 220 km at 12 s.

3.4 S-wave Data

3.4.1 Shear wave source

Analysis of the traces near the shotpoints indicates that the shear and compressional waves have a common source. However, White and Sengbush (1963) show that it is unlikely that shear waves could be produced by a large explosive source. It is therefore much more likely that the shear waves were produced by a conversion of compressional waves reflecting off the free surface. Fertig (1982) shows that this mechanism is capable of producing shear wave amplitudes comparable to those of compressional waves and points out that the reflected waves would appear to have been generated at the shot if the source depth is much less than the dominant wavelength. Since the dominant wavelength of the shear waves in this study was about 500 m, much larger than the 30 m shot depths, the shear wave arrivals were modelled as having originated at the shotpoint.

3.4.2 Modelling procedure

Since the quality of the shear wave data was not sufficient for independent structural modelling, the shear velocities were modelled using the layer boundaries of the P-wave model as constraints. A starting model was then constructed using those boundaries and the initial assumption that Poisson's ratio was 0.25. The value of Poisson's ratio for each layer was then adjusted until the resulting velocities gave a satisfactory travel-time fit.

3.4.3 The model

The shear wave model is shown in Figure 3.9. The sediments beneath shotpoint SP have been modelled in two packages: the upper two layers of the P-wave model, which are Mesozoic and younger, and a lower layer, which is predominantly Paleozoic. Poisson's ratio was found
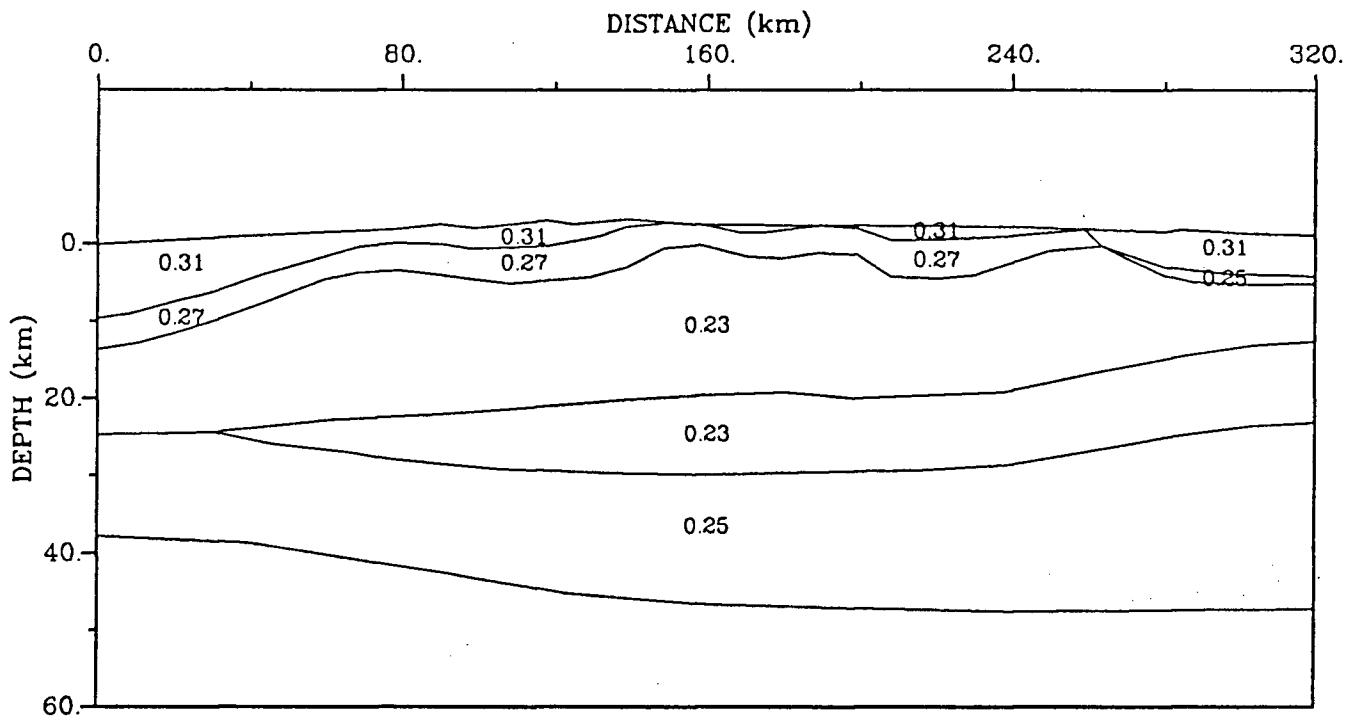
Figure 3.9: a) Shear wave model showing the boundaries used in modelling Poisson's ratio.
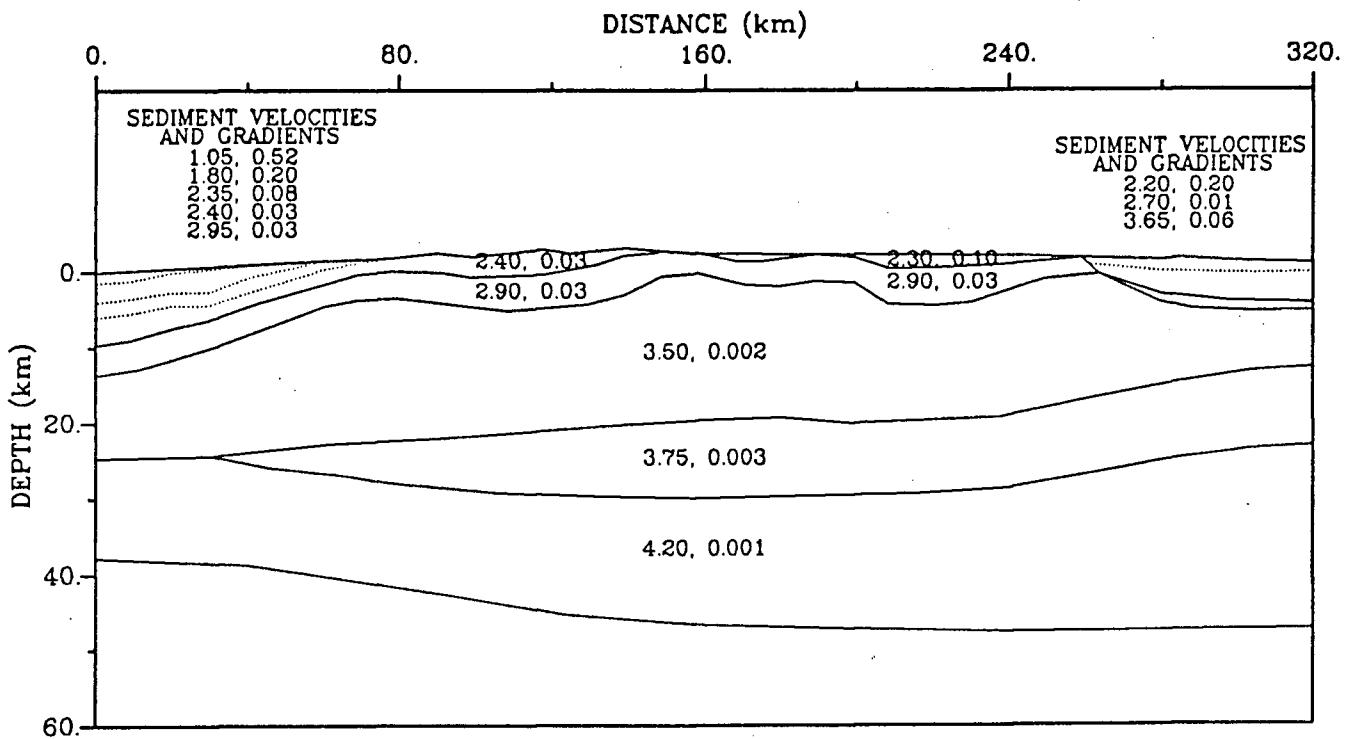

Figure 3.9: b) Shear wave model showing S-wave velocities (km/s) and gradients (s^{-1}) corresponding to the values of Poisson's ratio shown above.

to be 0.31 in the younger sediments and 0.27 in the Paleozoic sediments. The sediments

beneath EP also have a Poisson's ratio of 0.31, while the high velocity zone at the base of

the sediments has a value of 0.25. The upper crust was modelled as a single unit, without

internal reflectors, and was found to have a Poisson's ratio of 0.23. The mid crust also had a

value of 0.23, while the lower crust, which was also modelled without any internal reflectors,

had a value of 0.25. No mantle refractions or head waves from the Moho were observed in

the shear wave data, so mantle velocities could not be modelled.

3.4.4   Shot EP

Figure 3.10 shows the raypaths through the model from shotpoint EP, as well as the calculated

and observed travel-times. The fit to the data is very good, with most arrivals being within

the 200 ms error estimate. Since the starting model had travel time misfits over one second

for some of the arrivals from the sediments, the final model is a substantial improvement

over a constant crustal Poisson's ratio. Fortunately, most of the P-wave events which were

modelled had corresponding S-wave events, and as a result there were 86 travel-time picks

involved in the modelling. The first arrivals out to 300 km, about 20 km from EP, are

due to refractions from within the sediments, while refractions from the high velocity zone

at the base of the sedimentary sequence and head waves along the top of the crystalline

basement provide first arrivals to 170 km. The remaining first arrivals, out to 60 km, have

been modelled as head waves from the top of the lower crust. In addition to reflections from

the sediments, three major secondary events were modelled. The base of the upper crust

generated reflections between 280 km and 250 km, while reflections from the base of the

mid crustal layer were visible from 250 km to 160 km. The secondary arrivals between 140

km and 120 km have been modelled as a combination of reflections from the base of the mid

crust and reflections from the Moho. Reflections from the Moho are also present between

DISTANCE (KM)

Figure 3.10: a) Shear wave ray paths through the model from shot EP. The model boundaries are marked with heavier lines.

DISTANCE (KM)
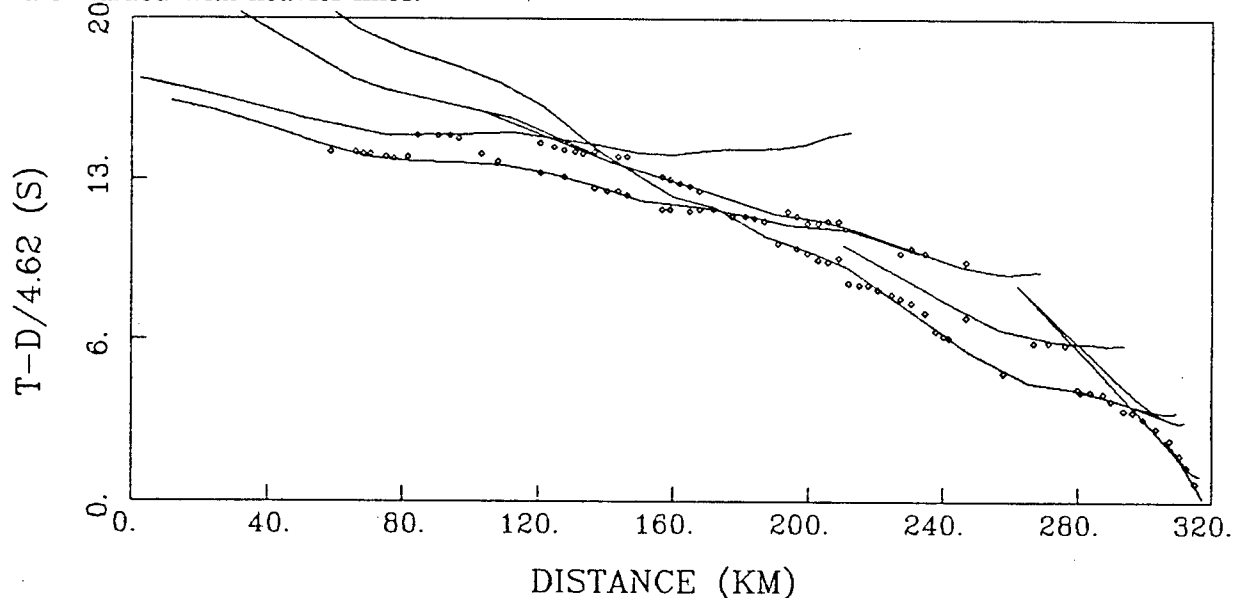
Figure 3.10: b) Observed travel-times for shot EP (0.2 s high diamonds) with calculated times (lines) for the model shown above.

100 km and 80 km.

3.4.5 Shot SP

Figure 3.11 shows the raypaths through the model from shotpoint SP, as well as the calculated and observed travel-times. The fit to the data is again excellent, with most of the first arrivals being within the estimated error of 200 ms. The secondary picks, particularly those between 100 km and 130 km, have not been modelled as accurately, but the picking errors for these arrivals were substantially higher than those for the primaries because of the relatively high amplitude reverberations following the first arrivals. The quality of this data set is not as good as that from shot EP and as a result only 38 picks were made. First arrivals out to about 25 km from the shotpoint have been modelled as refractions from within the sediments, while the first arrival picks from 80 km to 140 km were modelled as head waves along the top of the crystalline basement. In addition to reflections from within the sediments, two other secondary arrivals were modelled. The secondary arrivals between 100 km and 130 km, as well as those between 200 km and 210 km, have been modelled as reflections from the base of the upper crust, while the arrivals between 170 km and 220 km are reflections from the Moho. This event appears very clearly between 170 km and 200 km, corresponding to reflections from the same region of the Moho, between 105 km and 120 km, that produced strong P-wave reflections.

The unpicked event between 70 km and 140 km, approximately one second earlier than the picked shear arrivals (see Figure 2.9) is interpreted to be a P-S converted phase from the base of the sediment sequence. The apparent velocity of the event is consistent with the arrivals being shear wave refractions from the top of upper crust. The estimated error of the arrival time picks, however, makes it impossible to determine exactly where the P-S conversion takes place, though the one second difference between these arrivals and the
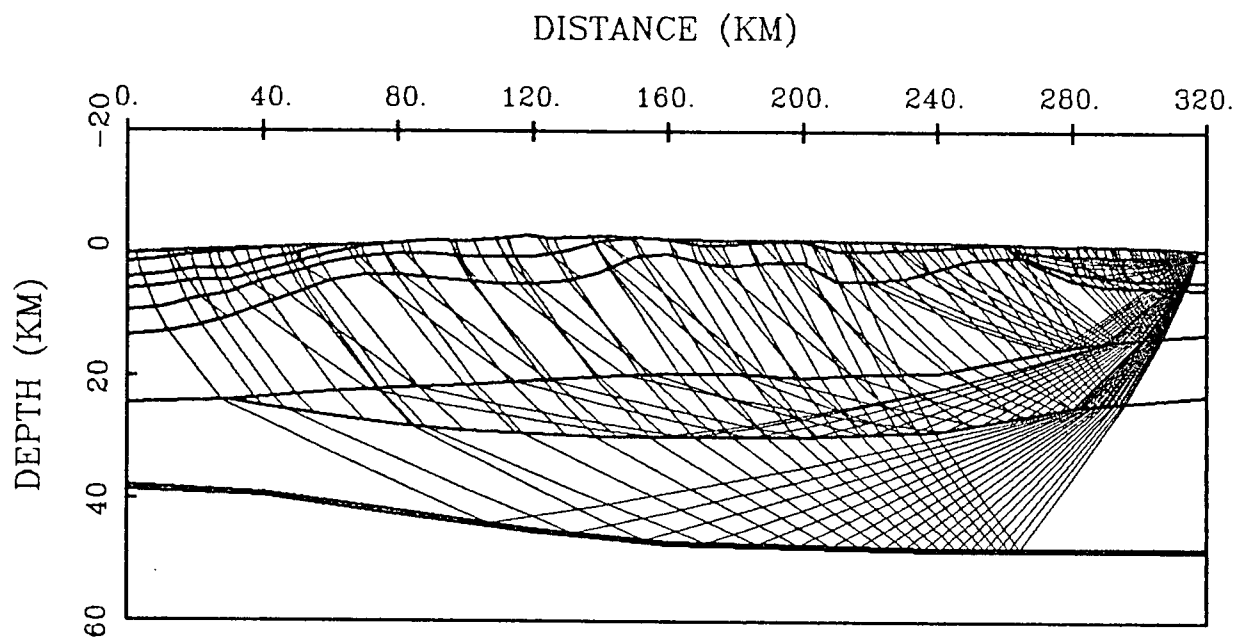
DISTANCE (KM)
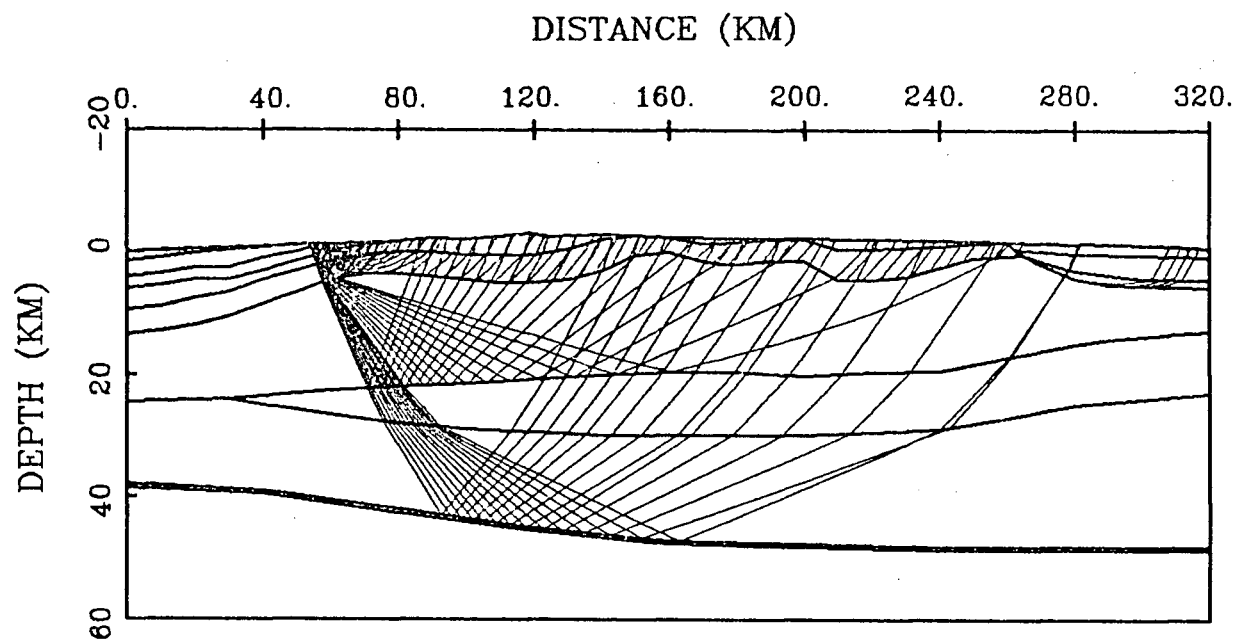
Figure 3.11: a) Shear wave ray paths through the model from shot SP. The model boundaries are marked with heavier lines.

DISTANCE (KM)
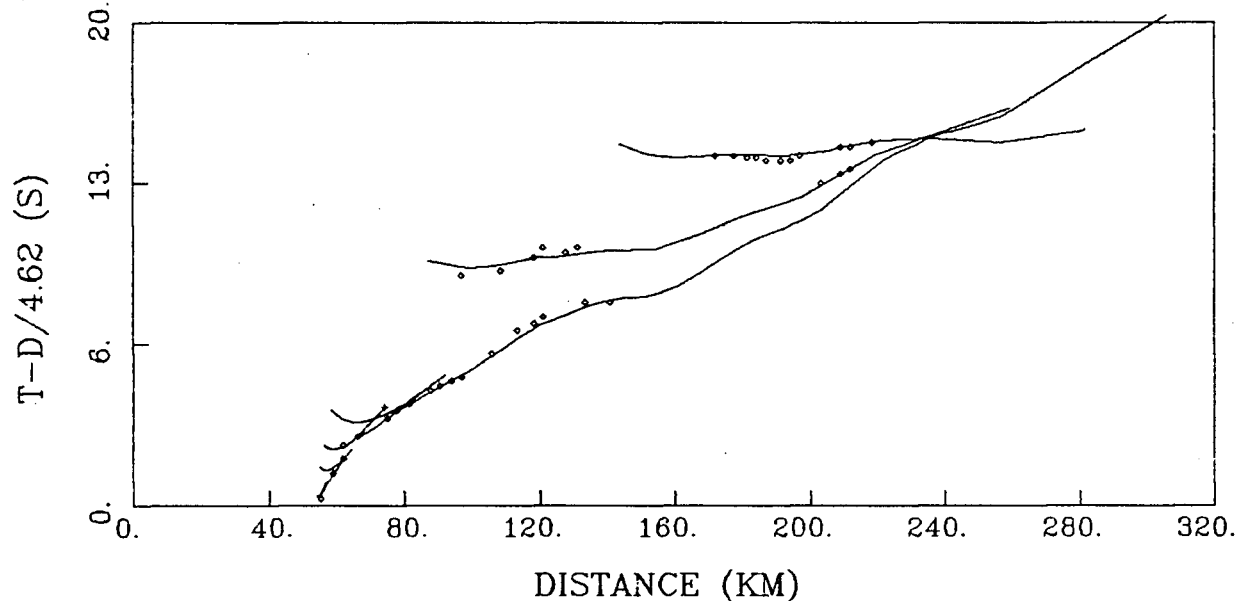
Figure 3.11: b) Observed travel-times for shot SP (0.2 s high diamonds) with calculated times (lines) for the model shown above.

SEDIMENTS	6.5 km	V_{av} = 4.89 km/s
UPPER CRUST	14.8 km	V_{av} = 5.93 km/s
MID CRUST	7.4 km	V_{av} = 6.32 km/s
LOWER CRUST	17.5 km	V_{av} = 7.08 km/s

Figure 3.12: Simple 1D model used in error calculations.

corresponding shear arrivals from the shot seems to indicate that the conversion occurred during transmission through the bottom sediment layer.

3.5 Error Analysis

The determination of error bounds on a 2D velocity model is a difficult problem. Since travel-time picks are the only observations from this data set for which we can reliably estimate errors, the uncertainties in the model parameters must be calculated in terms of their contribution to the travel-time errors. However, since the position of the boundaries and the velocity of the layers both contribute to the travel-time errors of the rays, the uncertainties in these quantities are interdependent. In order to determine the error bounds on any particular model parameter, it is therefore necessary to examine how a misfit produced by altering the parameter can be reduced by adjusting the other parameters. Due to the large number of model parameters, this method is not practical.

A common method of obtaining error estimates for seismic refraction models is to assume

that the parameters are somewhat independent. Each parameter is varied, while keeping all of the other parameters constant, in order to determine the variation which can be tolerated while still maintaining an acceptable fit (e.g. Zelt and Ellis, 1989). A slightly different approach was taken here. A simplified 1D model was constructed by averaging the velocities and thicknesses of the sedimentary sequence and the upper, mid and lower crustal layers (see Figure 3.12). Velocity errors for each layer were calculated by first assuming that the layer thicknesses were accurate and that the velocities of all of the other layers did not contribute to the error. The estimated travel-time error associated with the arrivals from the layer was then used to calculate the uncertainty in the velocity of a ray which travelled vertically down through the layer and then back.

Errors in layer thickness were calculated assuming the velocities were correct and that the travel-time errors for arrivals from each layer were due entirely to uncertainties in the thickness of the particular layer. Depth errors were then determined by summing the thickness errors down to each boundary. Table 3.1 shows the results of these calculations. Although this method does not take account of errors arising from the 2D nature of the original model, it does calculate maximum error estimates for the 1D model since it is based on the rays staying a minimum amount of time in each layer. Since the actual travel-time of the rays through the layers in the 2D model are longer, the 1D error estimates should be reasonable approximations for the 2D model. The estimates are very similar to those of Zelt and Ellis (1989).

These calculations are least likely to be accurate in the sediment layers where the complex structure makes the 1D analogy less likely to be valid, but travel-times for events turning in the sediments near the shotpoints are very accurately known, and thus the error estimates are quite good near the shotpoints. However, a problem does arise in the sediment basins on either side of the Aklavik Arch at the centre of the model, where there are no turning rays in the sediments. Head wave arrivals constrain the vertical travel-times through the basin,

Layer	Travel-time error estimates (s)	Velocity (km/s)	Depth to base (km)
Sediments	0.025	4.89 ± 0.05	6.5 ± 0.15
Upper Crust	0.050	5.93 ± 0.06	21.3 ± 0.4
Mid Crust	0.075	6.32 ± 0.20	28.7 ± 1.0
Lower Crust	0.100	7.08 ± 0.15	46.2 ± 1.7

Table 3.1: Error estimates for the 1D P-wave model.

Layer	Travel-time error estimates (s)	Velocity (km/s)	Poisson's Ratio
Sediments	0.10	2.66 ± 0.11	0.29 ± 0.02
Upper Crust	0.15	3.51 ± 0.12	0.23 ± 0.02
Mid Crust	0.20	3.74 ± 0.34	0.23 ± 0.04
Lower Crust	0.15	4.09 ± 0.14	0.25 ± 0.02

Table 3.2: Error estimates for the 1D S-wave model.

but, due to the potential trade off between velocity and depth, it is unlikely that the accuracy of the sediment P-wave velocities is any better than ± 0.2 km/s or that the accuracy of the depths to basement is better than ± 0.5 km.

Assuming the 1D analogy, the error calculations have several important ramifications. First, although the mid crustal layer is poorly constrained by the data, the data do indicate that such a layer is present with a velocity at least 0.13 km/s greater than the upper crust (6.12 km/s vs. 5.99 km/s). The thinning of this layer in the north also seems to be justified, although errors on the top and bottom of the layer indicate that it is not required to pinch out entirely, but may continue with a thickness of up to 1.4 km through the pinched out zone. The 11 km of crustal thinning beneath the Beaufort-Mackenzie Basin is also significant, since the depth to Moho is accurate to within 1.7 km.

The same method was also used for computing the error bounds on the shear wave velocities (see Table 3.2). The relative errors in Poisson's ratio are simply twice the sum of the relative errors of the P and S-wave velocities. Although the velocity errors are obviously higher than the P-wave errors due to the lower data quality, the high Poisson's ratio in the sediments contrasted with the low Poisson's ratio in the upper crust are significant. However, the low Poisson's ratio in the mid crust is not significant.

Chapter 4

DISCUSSION

4.1 Sediment Ages and Structure

This study has included the modelling of velocity structures within two distinct sedimentary sequences, one in the Beaufort-Mackenzie Basin at the northern end of the line and one in the Richardson Anticlinorium at the southern end. The Beaufort-Mackenzie Basin was modelled as a sediment package which increases in thickness to a maximum of 13.5 km beneath shotpoint MB (see Figures 3.1 and 3.2). The top three sediment layers are interpreted as being of Tertiary to Quaternary age, with a total thickness of up to 6 km. The base of this sequence marks the top of a low velocity zone ($\Delta v_p = -0.2\,km/s$) which may be associated with the middle Eocene unconformity described by Majorowicz and Dietrich (1989). Cretaceous and Jurassic sediments are contained in the underlying layer, to produce a total of 9.5 km of Mesozoic and younger sediments beneath shotpoint MB. The relatively high values for Poisson's ratio, 0.31, in these sediments are consistent with the results of Lash (1980) who found Poisson's ratios greater than 0.34 in clastic sediments of similar age in Texas. The lowest sedimentary layer is interpreted to be predominantly Paleozoic, possibly with some Mesozoic sediments at the top of the layer. The Rapid Depression, an extension of the Beaufort-Mackenzie Basin, contains up to 3 km of Mesozoic sediments and an additional 4 to 4.5 km of older sediments. There are no Cenozoic sediments present.

The Richardson Anticline, beneath shotpoint EP at the southern end of the line, was modelled as two near horizontal sedimentary layers having a total thickness of 5.5 km.

These are underlain by a high velocity layer approximately 1 km thick with velocities from 6.3 to 6.4 km/s. The composition of this layer is questionable. The few intrusions which have been observed in the surrounding area are all granitic (Norris, 1984), which would be expected to have velocities near 6.0 km/s (Holbrook et al., 1988). It is therefore unlikely that an intrusion could explain the high velocities. A more likely scenario is that the layer is composed of high velocity carbonates. Both the Proterozoic and early Paleozoic sediments in this area are known to include limestones and dolomites (Norris, 1984).

Unfortunately, the model resolution is weak between shotpoint SP and the Deception Fault. As a result, very little can be said about the structure of the Aklavik Arch except that the sedimentary basement has been uplifted 4.5 km beneath the White Uplift and 3 km beneath the Rat Uplift.

4.2 Crustal Structure and Composition

A number of observations can also be made about the crustal velocities. The low Poisson's ratio of 0.23 in the upper crust, as well as the compressional velocities near 6 km/s, indicate a quartz-rich granitic composition based on a comparison with the velocities discussed by Holbrook et al. (1988). The mid crustal layer also appears to be granitic, though the higher velocities (v_p = 6.3km/s, σ = 0.23) indicate a somewhat more mafic composition than that of the upper crust. The P-wave velocity (7.25 km/s) and Poisson's ratio (0.25 ± 0.02) of the lower crust are most consistent with a felsic to intermediate garnet granulite composition. However, this assumes that the lower crust has a fairly uniform composition. Serpa and de Voogt (1987) suggested that intrusion of mafic and ultramafic material into the lower crust may occur during crustal extension. This mixture could also explain the velocities seen here.

The depth to Moho of 38 km at the northern end of line is consistent with the interpretation of seismic reflection data on the eastern side of the Mackenzie delta (Cook et al., 1987) which

indicated a Moho depth of approximately 40 km beneath the edge of the Beaufort-Mackenzie Basin. The crustal thickness of 49 km beneath the Richardson Mountains is also reasonable, since greater thicknesses have been observed in the Rocky Mountains (Mereu et al., 1977: 54 km, Spence et al., 1977: 52–60 km), which are of similar age but greater topography.

The variable reflectivity of the Moho is not unexpected. Numerous studies have shown that the boundary between the lower crust and upper mantle is rarely a simple velocity discontinuity. Hale and Thompson (1982) noted that the Moho often appears to be a finely laminated transition zone, with the reflectivity being produced by the tuning of reflections from the various laminae. The data for this experiment recorded reflections from two segments of the Moho, one between 40 and 60 km and the other between 105 and 120 km, but no reflections were observed from elsewhere on the Moho. This may be due to variations in the thickness of the laminae or may indicate the presence of a high gradient transition zone.

4.3 Tectonic Implications

The most significant features of the model are the pinch out of the mid crustal layer and the substantial crustal thinning which occurs beneath the Rapid Depression at the northern end of the line. It is also notable that 9 km of the 11 km of thinning is within the lower crustal layer. This is consistent with the theory that this region is a passive rifted margin, comparable to the Atlantic margin. Several studies around the north Atlantic have observed similar phenomena. Reston and Blundell (1987), for example, proposed that a series of mid crustal reflectors beneath the edge of the North Sea Basin are from shear zones which developed as a result of lower crustal stretching accompanying rifting of the more brittle upper crust. Another study, based on the interpretation of wide angle reflection data from the northern Appalachians (Luetgert et al., 1987), constructed a very similar velocity model to the one of this study, which showed thinning accommodated primarily in the lower crust.

Haworth and Keen (1979) also suggested that the rifting of the Atlantic was accomplished through block faulting in the upper crust and plastic flow in the lower crust. Keen (1985) suggested that there are several different dynamic models which can explain the rifting process, but they all involve a two layered lithosphere, with the upper crust deforming by brittle failure while the lower crust and remaining lithosphere undergo ductile deformation.

Although the velocity model developed here shows no evidence of upper crustal rifting, the lateral resolution of this model is probably not sufficient to see the near vertical faulting associated with rifting. It is possible that some of the dipping boundaries modelled at the northern end of line, particularly the sedimentary basement of the Beaufort-Mackenzie Basin, are actually rifted segments which have been smoothed by the modelling process. Seismic reflection studies off the northern coast of Alaska (Grantz and May, 1983) and over the Mackenzie Delta (Cook et al., 1989) have observed upper crustal structures which appeared to be due to rifting.

The composition of the lower crust predicted by the velocity model is either felsic to intermediate garnet granulite or possibly mafic to ultramafic intrusions in a felsic matrix. As previously noted, Serpa and de Voogt (1987) suggested that mafic to ultramafic material may intrude into the lower crust during the extension associated with the development of a passive margin. Since the rifting process could subject the margin to high pressure and high temperature metamorphism, a granulitic lower crustal composition would also be consistent with this being a passive margin.

Haworth and Keen (1979) also noted that the continental crust along the transform margin of the southern Grand Banks is not substantially thinned with the continent-ocean transition being very abrupt. The velocity model developed here suggests that thinning is fairly gradual, while gravity modelling by Sobczak (1974) indicates that the continental crust continues to thin under Mackenzie Bay to a thickness of less than 25 km at the edge of the shelf. This indicates that it is unlikely that the edge of the Beaufort Sea is a transform margin as some

tectonic models have suggested.

4.4 Summary

This study has constructed a model for the shear and compressional velocities beneath the Richardson Mountains in the northern Yukon. The main features of this model include:

1. a very complicated sediment structure, including three major basement highs, near model distances of 60, 160 and 260 km. The first marks the boundary between the Rapid Depression and the remainder of the Beaufort-Mackenzie Basin, the second is produced by the Aklavik Arch, while the third correlates with the edge of the Richardson Anticlinorium.

2. no significant crustal velocity or thickness variations across the Kaltag Fault.

3. weak resolution of upper crustal velocities near the Aklavik Arch. Very little can therefore be said about the deep structure of the uplifts.

4. a high velocity zone (6.35 km/s) at the base of the sediments beneath shot EP which is interpreted to be late Proterozoic or early Paleozoic carbonates.

5. a granitic upper crust (v_p = 5.95 km/s, σ = 0.23) having an average thickness of approximately 15 km.

6. a slightly more mafic mid crustal layer (v_p = 6.3 km/s, σ = 0.23) which has a thickness of 10 km in the south but pinches out beneath the Rapid Depression.

7. a fairly high velocity (v_p = 7.25 km/s, σ = 0.25) lower crust which has an average thickness of 18 km, but thins by 9 km over the northern half of the line. The velocities suggest an intermediate granulite composition or a mixed composition of mafic to ultramafic intrusions in a more felsic matrix.

8. a deep (50 km) Moho beneath the Richardson Mountains which shallows to 40 km under the Beaufort-Mackenzie basin.

The velocity model is similar to models from the Atlantic margin of North America, indicating that coast of the Beaufort Sea is likely a passive margin. This would make the fault based tectonic models for the evolution of the Canada Basin improbable.

4.5 Experiment Limitations and Recommendations for Future Studies

The weakest part of the model developed here is the lack of control on the velocity structure of the sedimentary sequence between shotpoint SP and the Deception Fault. As a result, the upper crustal resolution between the Rapid Depression and the Deception Fault is weak. There are several things which could be done to help this. Additional refraction data for shotpoints located between SP and EP would be very useful to resolve shallow structure around the Aklavik Arch, while a reduced receiver spacing would significantly improve the spatial resolution.

In addition, the modelling of the existing gravity data may add useful constraints. Extension of the line 50 to 100 km to the north would provide a much more complete picture of the continent-ocean transition. A seismic reflection study may also be very useful, especially for constraining sediment structure and for locating rifts. It may also help to constrain layer boundaries.

REFERENCES

Birch, F., 1964. Density and composition of mantle and core. *J. Geophys. Res., v. 69*, p. 4377-4388.

Červený, V., Molotkov, I. and Pšenčík, I., 1977. *Ray method in seismology.* University of Karlova, Prague, Czechoslovakia, 214 p.

Christensen, N.I. and Szymanski, D.L., 1988. Origin of reflections from the Brevard Fault Zone. *J. Geophys. Res, v. 93*, p. 1087-1102.

Churkin, M.J. and Trexler, J.H., 1980. Circum-Arctic plate accretion – isolating part of a Pacific plate to form the nucleus of the Arctic Basin. *Earth Planet. Sci. Lett., v. 48*, p. 356-362.

Cook, F.A., Coflin, K.C., Lane, L.S., Dietrich, J.R. and Dixon, J., 1987. Structure of the southeast margin of the Beaufort-Mackenzie Basin, from crustal seismic-reflection data. *Geology, v. 15*, p. 931-935.

Cormier, V.F. and Spudich, P., 1984. Amplification of ground motion and waveform complexity in fault zones: examples from the San Andreas and Calaveras faults. *Geophys. J. R. astron. Soc., v. 79*, p. 135-152.

Dixon, J., Dietrich, J.R., McNeil, D.H., McIntyre, D.J., Snowden, L.R. and Brooks, P., 1985. *Geology, biostratigraphy and organic geochemistry of Jurassic to Pleistocene strata, Beaufort-Mackenzie area, northwest Canada.* Course Notes, Canadian Society of Petroleum Geologists, Calgary, Alberta, 65 p.

Dutro, J.T. 1981, Geology of Alaska bordering the Arctic Ocean. In: Nairn, A.E.M. (Editor), *The Ocean Basins and Margins, v. 5*, p. 21-36.

Fertig, J., 1984. Shear waves by an explosive point-source: the earth surface as a generator of converted P-S waves. *Geophys. Prosp., v. 32*, p. 1-17.

Grantz, A., Eittreim, S. and Dinter, D.A., 1979. Geology and tectonic development of the continental margin north of Alaska. *Tectonophysics, v. 59*, p. 263-291.

Grantz, A. and May, S.D., 1983, Rifting history and structural development of the continental margin north of Alaska. In: Watkins, J.S. and Drake, C.L. (Editors), Studies in

Continental Margin Geology, *Am. Assoc. Pet. Geol. Mem. 35*, p. 77-100.

Hale, L.D. and Thompson, G.A., 1982. The seismic reflection character of the continental Mohorovičić discontinuity. *J. Geophys. Res., v. 87*, p. 4625-4635.

Haworth, R.T. and Keen, C.E., 1979. The Canadian Atlantic margin: a passive continental margin encompassing an active past. In: C.E. Keen (Editor), Crustal Properties across Passive Margins. *Tectonophysics, v. 59*, p. 83-126.

Herron, E.M., Dewey, J.F. and Pitman, W.C. III, 1974. Plate tectonics model for the evolution of the Arctic. *Geology, v. 2*, p. 377-380.

Holbrook, W.S., Gajewski, D., Krammer, A. and Prodehl, C., 1988. An interpretation of wide-angle compressional and shear wave data in southwest Germany: Poisson's ratio and petrological implications. *J. Geophys. Res., v. 93*, p. 12081-12106.

Irving, E., 1977. Drift of the major continental blocks since the Devonian. *Nature, v. 270*, p. 304-309.

Jones, 1980. Evidence from Canada and Alaska on plate tectonic evolution of the Arctic Ocean Basin. *Nature, v.285*, p. 215-217.

Keen, C.E., 1985. The dynamics of rifting: deformation of the lithosphere by active and passive driving forces. *Geophys. J. R. astr. Soc., v. 80*, p. 95-120.

Lane, L.S., 1988. The Rapid Fault Array: a foldbelt in Arctic Yukon. In: *Current Research, Part D, Geological Survey of Canada, Paper 88-1D*, p. 95-98.

Lash, C.C., 1980. Shear waves, multiple reflections, and converted waves found by a deep vertical wave test (vertical seismic profiling). *Geophysics, v. 45*, p. 1373-1411.

Luetgert, J.H., Mann, C.E. and Klemperer, S.L., 1987. Wide angle reflections in the northern Appalachians. *Geophys. J. R. astr. Soc., v. 89*, p.183-188.

Mackay, J.R., 1967. Permafrost depths, lower Mackenzie Valley, *Arctic, v. 20*, p.21-26.

Majorowicz, J.A. and Dietrich, J.R., 1989. Comparison of the geothermal and organic maturation gradients of the central and southwestern Beaufort-Mackenzie Basin, Yukon and Northwest Territories. In: *Current Research, Part G, Geol. Surv. of Can., Paper 89-1G*, p. 63-67.

Mereu, R.F., Majumdar, S.C. and White, R.E., 1977. The structure of the crust and upper mantle under the highest ranges of the Canadian Rockies from a seismic refraction survey. *Can. J. Earth Sci., v.14*, p. 196-208.

Mitchell, B.J. and Hwang, H.J., 1987. Effect of low Q sediments and crustal Q on Lg attenuation in the United States. *Bull. Seism. Soc. Am., v. 77*, p. 1197-1210.

Norris, D.K., 1974. Structural geometry and geological history of the northern Canadian Cordillera. In: *Proceedings, Can. Soc. of Explor. Geophys., 1973 National Convention*, p. 18-45.

Norris, D.K., 1984. Geology of the northern Yukon and northwestern District of Mackenzie. Geol. Surv. of Can., Map 1581A, scale 1 : 500 000.

Peach, R., 1988. *A preliminary report on the study of sediment compaction and overpressures in the Beaufort-Mackenzie Basin using sonic logs*. Institute of Sedimentary and Petroleum Geology, Calgary, 210 p.

Reston, T.J. and Blundell, D.J., 1987. Possible mid-crustal shears at the edge of the London Platform. *Geophys. J. R. astr. Soc., v. 89*, p. 251-258.

Serpa, L. and de Voogt, B., 1987. Deep seismic evidence for the role of extension in the evolution of continental crust. *Geophys. J. R. astr. Soc., v. 89*, p. 55-60.

Sobczak, L.W., 1975. Gravity and deep structure of the continental margin of Banks Island and Mackenzie Delta. *Can. J. of Earth Sci., v. 12*, p. 378-394.

Spence, G.D., Clowes, R.M. and Ellis, R.M., 1977. Depth limits on the M discontinuity in the southern Rocky Mountain Trench. *Bull. Seism. Soc. Am., v. 67*, p. 543-546.

Spencer, C. and Asudeh, I., 1987. *Lithoprobe Data Storage*. Internal Report, Seismology and Electromagnetism Section, Lithosphere and Canadian Shield Division, Geological Survey of Canada, 27 p.

Stephenson, R.A., Zelt, B.C., Asudeh, I., Forsyth, D.A., Spencer, C. and Ellis, R.M., 1989. *Acquisition of regional seismic refraction data in the Mackenzie Delta-Southern Beaufort Sea-Northern Yukon Area, 1987*. Open file Report # 2058, Geologic Survey of Canada, 65 p.

Sweeney, J.F, Weber, J.R. and Blasco, S.M., 1982. Continental ridges in the Arctic Ocean: LOREX constraints. In: G.L. Johnson and J.F. Sweeney (Editors), Structure of the Arctic. *Tectonophysics, v. 89*, p. 217-237.

Taylor, P.T., Kovacs, L.C., Vogt, P.R. and Johnson, G.L., 1981. Detailed aeromagnetic investigation of the Arctic Basin. *J. Geophys. Res., v. 86*, p. 6323-6333.

Vogt, P.R., Taylor, P.T., Kovaks, L.C. and Johnson, G.L., 1982. The Canada Basin: aeromagnetic constraints on structure and evolution. In: G.L. Johnson and J.F. Sweeney (Editors), Structure of the Arctic. *Tectonophysics, v. 89*, p. 295-336.

Weber, J.R. and Sweeney, J.F 1985. Reinterpretation of the morphology and crustal structure in the central Arctic Ocean Basin. *J. Geophys. Res., v. 90*, p. 663-677.

White, J.E. and Sengbush, R.L., 1963. Shear waves from explosive sources. *Geophysics, v. 28*, p. 1001-1019.

Young, F.G., Myhr, D.W. and Yorath, C.J., 1976. Geology of the Beaufort-Mackenzie Basin. *Geological Survey of Canada, Paper 76-11*, 65 p.

Zelt, C.A. and Ellis, R.M., 1988. Practical and efficient ray tracing in two-dimensional media for rapid travel-time and amplitude modelling. *Can. J. Explor. Geophys., v. 24*, p. 16-31.

Zelt, C.A. and Ellis, R.M., 1989. Seismic structure of the crust and upper mantle in the Peace River Arch region, Canada. *J. Geophys. Res., v. 94*, p. 5729-5744.

Zelt, C.A. and Ellis, R.M., 1990. Crust and upper mantle Q from refraction data: Peace River Arch region. *Can. J. Earth Sci.*, (in press).